REPORT ON PROGRESS

A review of progress in single particle tracking: from methods to biophysical insights

To cite this article: Carlo Manzo and Maria F Garcia-Parajo 2015 *Rep. Prog. Phys.* **78** 124601

IOP Publishing Reports on Progress in Physics
Rep. Prog. Phys. **78** (2015) 124601 (29pp) doi:10.1088/0034-4885/78/12/124601

Report on Progress

A review of progress in single particle tracking: from methods to biophysical insights

Carlo Manzo[1] **and Maria F Garcia-Parajo**[1,2]

[1] ICFO-Institut de Ciencies Fotoniques, Mediterranean Technology Park, 08860 Castelldefels (Barcelona), Spain
[2] ICREA-Institució Catalana de Recerca i Estudis Avançats, 08010 Barcelona, Spain

E-mail: carlo.manzo@icfo.es and maria.garcia-parajo@icfo.es

Invited by Maciej Lewenstein

Received 23 March 2014, revised 6 July 2015
Accepted for publication 15 July 2015
Published 28 October 2015

Abstract

Optical microscopy has for centuries been a key tool to study living cells with minimum invasiveness. The advent of single molecule techniques over the past two decades has revolutionized the field of cell biology by providing a more quantitative picture of the complex and highly dynamic organization of living systems. Amongst these techniques, single particle tracking (SPT) has emerged as a powerful approach to study a variety of dynamic processes in life sciences. SPT provides access to single molecule behavior in the natural context of living cells, thereby allowing a complete statistical characterization of the system under study. In this review we describe the foundations of SPT together with novel optical implementations that nowadays allow the investigation of single molecule dynamic events with increasingly high spatiotemporal resolution using molecular densities closer to physiological expression levels. We outline some of the algorithms for the faithful reconstruction of SPT trajectories as well as data analysis, and highlight biological examples where the technique has provided novel insights into the role of diffusion regulating cellular function. The last part of the review concentrates on different theoretical models that describe anomalous transport behavior and ergodicity breaking observed from SPT studies in living cells.

Keywords: single molecule fluorescence, transport in living systems, cell biophysics, anomalous diffusion, nonergodicity

(Some figures may appear in colour only in the online journal)

1. Introduction

Deciphering the complex interactions between myriads of different molecules expressed in a single cell has been a biology quest for many decades. Microscopy studies have revealed that cellular components, ranging from lipids to proteins on the cell surface, and intracellular organelles and DNA inside the cell nucleus, distribute in a highly non-homogenous fashion, both in space and time. Moreover, this organization appears highly dynamic at multiple spatial scales and responds to different biochemical and mechanical inputs. Importantly, the highly orchestrated and dynamic organization of cellular components is essential for many biological processes, including nuclear organization and signaling in cell division, differentiation, cell adhesion and migration. Having access to the mobility of the components that underlie the dynamic organization

of the cell is therefore crucial for understanding living systems on a microscopic mechanistic basis. It is noteworthy that not only biologists are making great progress in elucidating cell complexity, geared by the continuous development of advanced experimental techniques, but also physicists are playing an increasingly important role in the field. Indeed, the possibility of visualizing and resolving individual molecules in the natural context of living cells is translating into a more quantitative and accurate description of the spatiotemporal dynamic processes controlling cell function. Not surprisingly, therefore, physicists are being attracted to biology, contributing to the development of technology and novel tools for data analysis on the one hand, but also, importantly, providing comprehensive models that get us closer to understanding molecular transport and behavior in cells and their responses to the environment. The blending of biology with physics is therefore expected to reveal many of the molecular as well as physical mechanisms underlying the enormous complexity of living cells. Central to these advances is the development of non-invasive techniques capable of visualizing dynamic processes with ultimate sensitivity and high spatiotemporal resolution. One of these techniques is single particle tracking (SPT). As a preface to SPT, we briefly describe below some related techniques and provide a short overview on how SPT has evolved since its first application to study biological specimens in the mid 1980s.

1.1. Key enabling techniques to access dynamics in living cells: a brief description

A wealth of experimental techniques has been developed in recent decades for measuring dynamic processes in living systems. One of the most widespread techniques used by biologists for nearly four decades is fluorescence recovery after photobleaching (FRAP) [1, 2]. Although initially used to study the mobility of lipids and proteins in the cell membrane [3], FRAP can be also applied to study protein dynamics in the cytoplasm or cellular structures within the cell [1, 2]. The principle of FRAP is the selective switch off, by a photophysical process called photobleaching, of the fluorescence of labeled molecules in a given region of the sample. The mobility of the molecules is then measured from the recovery of the fluorescence in the bleached region as a function of time. The kinetics of the recovery depends on the mobility from the labeled molecules from other regions of the sample to the photobleached area, providing information on the diffusion of the molecules of interest as well as separating and quantifying mobile and immobile fractions.

Another powerful method to gain information on the dynamics of molecules in living cells is fluorescence fluctuation spectroscopy, including fluorescence correlation spectroscopy (FCS) [4–6] and image correlation spectroscopy (ICS) [7–9]. In general, these techniques analyze the fluctuations of the fluorescence intensity that arise from the passage of a dilute number of labeled molecules over the illumination volume, commonly achieved under confocal or two-photon excitation. The analysis provides the average number of the fluorescent molecules and the average diffusion time, so that in principle, both the concentration and size of the molecules can be determined. The size of the molecule can be determined by extracting its hydrodynamic radius from the measured diffusion coefficient using the Stokes–Einstein equation [4–6]. Although FRAP and FCS have the sufficient temporal resolution (below milliseconds) to monitor fast dynamic processes, their spatial resolution is limited by diffraction. As such, these techniques provide an ensemble time average of the dynamics of the molecules under study. Nanoscale heterogeneities within the cell that affect the diffusion of the molecules, and/or short-lived molecular interaction events are in general not accessible with these methods. Of note are two super-resolution techniques (stimulated emission depletion microscopy (STED) and near-field scanning optical microscopy (NSOM) that provide excitation volumes smaller than those established by diffraction and have allowed FCS recording of individual molecules on nanoscale regions (~50 nm in size) of living cell membranes [10, 11]. Moreover, several nanophotonic approaches (subwavelength aperture nanostructures and photonic antennas) are currently being developed to restrict excitation to nanoscale volumes, while enabling the detection of individual diffusion events in biological samples. Although these techniques are still in their infancy they hold great promise for future live cell applications (see [12–14] for recent reviews on this technology).

A different approach that combines high spatial and temporal resolution is single particle tracking (SPT), which is the main focus of this review. SPT provides information not available to FRAP and other methods that are based on the behavior of large ensembles of molecules. This is because SPT locates each individual particle with nanometric precision and measures its individual dynamics as a function of time.

1.2. The continuous evolution of SPT

The history of SPT dates to the mid-1980s, when Brabander and colleagues first showed that gold nanoparticles, as small as 40 nm in size, could be visualized on the surface of living cells by optical means [15, 16]. Initially called 'nanovid microscopy', the method relied on the sparse use of colloidal gold particles, rigidly attached to the biomolecule of interest. In the ideal situation, only a single biomolecule is attached to an individual gold particle. Because of their large Rayleigh intensity scattering, the spatial coordinates of the center positions of individual particles could be retrieved with precision at the level of nanometers from the recording at successive times using video enhanced differential interference contrast (DIC) microscopy [15]. This simple methodology allowed for the first time tracking kinesin-driven movements with nanometer-scale precision [17] and opened the field of tracking individual molecules in the cell membrane [18, 19]. Instead of using gold particles, large latex, polystyrene or silica particles with sizes ranging between 200 nm to 1 μm in diameter can also be imaged and then tracked using standard optical microscopy. Over the years, SPT together with the development of various molecular targeting strategies, data processing and modeling methods have been instrumental to study, among others, the heterogeneous and dynamic organization

of the plasma membrane (see [20] for one of the earliest comprehensive reviews on SPT). Given the simplicity of the technique in terms of implementation, numerous groups in the world dedicated their efforts to developing suitable algorithms for reconstructing trajectories and analyzing diffusion and flow in two- and three-dimensional systems (see the recent review [21]).

The major advantage of SPT using these types of reporters is their stability, since they not exhibit photobleaching or biodegradation, they therefore have the ability to probe individual biomolecules for long periods of times (even minutes), with high temporal resolution (frame rates up to 40 kHz [22] and excellent spatial localization precision (1–10 nm) due to their large scattering cross-section. However, their bulky sizes also put severe constraints on the biological process to be observed and might induce serious artifacts (to be discussed in more detail in section 2). Reduction of the particle size is troubled by the fact that Rayleigh scattering decreases as the sixth power of the particle diameter [23], thus prohibiting the detection of particles smaller than 30–40 nm using standard optical microscopy methods. A major breakthrough in fluorescence microscopy occurred in 1993, when individual molecules could be detected at room temperature by means of fluorescence [24]. Soon after that, SPT was implemented by replacing single particles with single fluorescent molecules or fluorescent proteins [25–27]. Since then the field has witnessed an explosion in terms of different optical implementations, algorithms for trajectory reconstruction and data analysis, physical models, and, importantly, it has led to new discoveries in biology.

SPT by means of fluorescence (also known as single dye tracing (SDT) or single molecule tracking (SMT)) took off in 1996, when the methodology was developed to visualize the motion of individual lipids on synthetic membranes using organic dyes [28], and later in 2000 to visualize the motion of signaling receptors and lipids on the surface of living cells [25, 29]. Over the years, the technique has been used to study a vast number of different systems in living cells, including dynamic processes on the cell surface (see recent reviews [30–32]), gene expression [33, 34], and 3D single dye tracking in the nucleus and cytosol of individual cells [31, 35–37] (see also section 4). Unfortunately, the trajectory length and spatial position precision of SPT by means of fluorescent reporters is typically restricted to a few seconds and to 20–50 nm, respectively [31, 38, 39]. This lower performance compared to non-fluorescent reporters has its origin in the reduced number of photons a fluorescent molecule can emit before photodissociation (between 10^5 to 10^6, depending on the molecule used) and in the autofluorescence of the cell at the probe's excitation wavelength.

The bottleneck of the rapid photobleaching of fluorescent molecules can be overcome by the use of semiconductor nanocrystals, also known as quantum dots (QDs) as alternative SPT reporters. In 2003, Dahan and co-workers followed for the first time the diffusion dynamics of glycin receptors in living cells using QD tracking [40]. Since then, the applications of QDs for SPT in living cells have been enormous, with particular emphasis on the investigation of processes at the level of the cell membrane (reviewed in [30, 31, 41, 42], but also intracellularly (reviewed in [31, 43, 44]), and more recently on brain slices [45].

Interestingly, the remarkable evolution of SPT has not only brought extraordinary (and somewhat unexpected) understanding to biology but has also resulted in an exquisite single molecule tool to explore the complexity of living systems from a physics perspective. In particular, two major findings from SPT experiments have triggered the interest of theoreticians and statistical physicists. First, although Brownian motion has been traditionally considered as one of the pillars of biological and soft condensed matter physics, a major observation in almost (if not all) SPT experiments (somewhat also inferred from other experimental techniques mentioned above) is that the diffusive motion of molecules in living cells is anomalous (reviewed in [20, 38, 46]). Anomalous transport has therefore received increasing attention in recent years with the development of a diversity of theoretical descriptions of the phenomena (for a recent review see [46] and section 5). Second, a more intriguing observation made only recently, but strongly connected to anomalous transport, is that diffusion processes in living cells are in general nonergodic, i.e. the time and ensemble averages are different [47–49]. Since SPT removes ensemble averaging, the diffusion of a single molecule can be followed for a long observation time, acquiring temporal-average information of the process. At the same time, many individual molecules can be observed and analyzed, so that spatial-average information is also available. Recent SPT experiments in living cells have demonstrated that time averages might vary from molecule to molecule, so that spatial and time averaging are not equivalent, breaking one of the hallmark hypotheses of statistical physics: ergodicity [50–53]. In section 5 of this review we discuss the development of new theoretical tools to interpret ergodicity-breaking in living cells and potential implications in terms of cellular function.

This review is structured as follows: in section 2 we describe the foundations for SPT paying particular attention to the different types of reporters and strategies for their attachment to the biomolecule to be tracked. We then elaborate on different technical implementations, together with latest technological advancements in the field. In section 3 we focus on data analysis algorithms to interpret trajectories from SPT images. These algorithms are separated into two main blocks: the first set of algorithms is focused on localizing the center positions of the probes used for SPT and the linking of the coordinates to generate trajectories that faithfully describe the movement of the particle. The second set of algorithms is focused on interpreting and analyzing these trajectories to determine parameters such as type of diffusion, diffusion coefficients, velocities, regions of entrapment, etc. Section 4 highlights some prominent examples on how SPT has advanced our understanding in cell biology, focusing mainly on studies of living cell membranes, as well as briefly reviewing examples where SPT has been essential for studying virus uptake, internalization and infection in living cells, and processes of gene transcription. Finally, in section 5 we concentrate on different theoretical models currently being developed to interpret

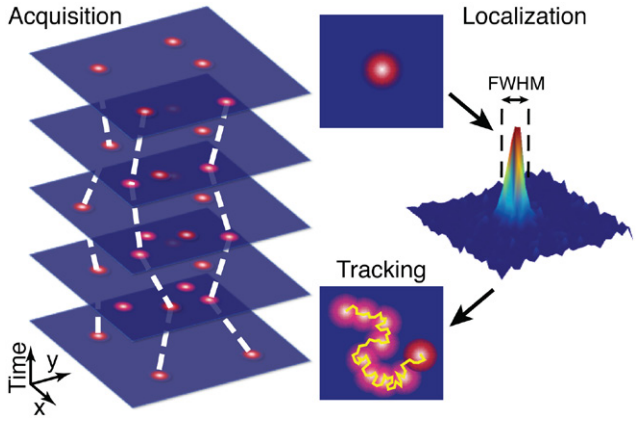

Figure 1. Schematic representation of SPT. In the acquisition step a series of images is taken, containing a sparse number of labeled molecules (red spots). Typical movies contain between hundreds to thousands of images recorded with a high-speed camera. In the localization step, the fluorescence image at a given time is analyzed to retrieve the positions of the particles. The positional accuracy ultimately depends on the full-width-at-half-maximum (FWHM) of the PSF, the number of photons collected from the emitter and the different sources of noise from the experiment. After repeating the localization step on a time series of images, the positions are linked to generate trajectories that track the motion of the particle (see also the white dashed lines on the acquisition images where individual particles are linked as a function of time).

SPT measurements in living cells, with a particular focus on anomalous transport and nonergodic behavior.

2. Technical implementation and the latest technological developments

2.1. The basics

The essence of SPT is schematically described in figure 1. As already mentioned in the introduction, SPT relies on the use of a nanoscopic reporter (gold nanoparticle, QD or fluorescence molecule) attached to the biomolecule of interest. The motion of the reporter is then imaged by optical microscopy and analyzed using imaging processing methods. The resulting trajectories provide direct access to the full statistics of spatial displacements, allowing for evaluation of physical properties, such as diffusion, velocity, transient interaction, trapping, etc as a function of time and space. The spatial and temporal resolutions and the total observation times are determined to a large extent by the photo-physical properties of the reporter, detector speed and signal-to-background considerations of the entire experiment (see below in this section).

The heart of the method is based on the fact that the image of a single point object acquired with an optical microscope will appear in the detector as a diffraction-pattern with a shape of concentric rings having decaying intensities as the distance from the center increases. The central ring, known as the Airy disk, contains most of the intensity and its profile can be approximated by a 2D spatial Gaussian,

$$I(x,y) \approx I_0 \exp\left\{-\frac{(x-x_0)^2}{2w^2}\right\} \exp\left\{-\frac{(y-y_0)^2}{2w^2}\right\}, \quad (1)$$

where I_0 is the intensity at the center of the disk and w is the standard deviation of the intensity profile, also known as the point spread function (PSF) of the microscope. Because of diffraction, the full-width-at-half-maximum (FWHM):

$$\mathrm{FWHM} = w\sqrt{8\log(2)} \approx \lambda/(2\mathrm{NA}), \quad (2)$$

where λ is the wavelength of the excitation light, and NA is the numerical aperture of the objective. Hence, the diffraction limit of light implies that two objects cannot be resolved individually if their mutual distance is smaller than the FWHM. For visible light and a NA of 1.3, the FWHM is around 250 nm. On the other hand, for distances larger than the FWHM, the different point objects will appear in the detector as distinguishable intensity spots and their centroid positions can be determined by fitting the intensity profile with a 2D-Gaussian function. Hence, a positional precision far beyond the optical resolution, down to a few nanometers, is obtainable. Importantly, this condition implies *per se* the use of sparse labeling conditions so that individual intensity spots are always well separated in space. Therefore, only a sub-set of the biomolecules of interest can be investigated at each given experimental condition.

By acquiring hundreds to thousands of images (using acquisition rates ranging from 10 to 40 000 Hz), the centroid positions of each single reporter can be subsequently linked between frames to generate trajectories that describe the motion of each individual reporter as a function of time (figure 1). The resulting trajectories can be analyzed for their type of motional behavior using different approaches, although the most widely used quantity is the mean-square-displacement (MSD) as a function of the time lag. The MSD describes the average of the square distance between the reporter's start point and its end position for all time lags of a certain duration within one trajectory. More comprehensive methods to analyze single trajectories are described in section 3 of this review.

The usefulness of the trajectories to describe a given dynamic process depends on the spatial localization accuracy and precision to identify the centroid positions of the reporter, the temporal resolution of the instrument and the experimental observation time. The localization precision is essentially a statistical indetermination, given by the number of photons forming the image and by the sources of noise, such as photon noise (the stochasticity of photon emission), pixelation noise and background noise, the latter including readout error, dark-count noise, and sample autofluorescence from the sample. Localization accuracy is not affected by shot noise but can be induced by other factors, such as anisotropic emission, detector noise, probe size and linkers. In practice, both the localization precision and accuracy will influence the exact reconstruction of the trajectory mobility since they ultimately determine how accurate the center position of the reporters can be asserted (see also section 3.3). Typical localization indeterminations range from 1 nm for gold particles and polystyrene beads, to about 10–15 nm for QDs and somewhere between 20 to 50 nm for fluorescent molecules.

The temporal resolution is essentially given by the speed of the detector and the integration times required to collect enough photons. Modern cameras can reach speeds higher than 1000 frames s^{-1}, with high sensitivity and very low read-out noise. However, when reaching these high speeds, the main restrictive factor again becomes the number of photons collected from the reporter. Finally, the experimental observation time is limited by the photostability of the reporter and/or drift of the instrument. It can typically last for tens of minutes in the case of gold and beads, to several minutes for QDs, and decreasing very rapidly to a couple of seconds in the case of fluorescent molecules. Overall, it is worth realizing that spatial localization precision, temporal resolution and observation times are all coupled to the number of photons from the reporter [39]. This is particularly critical when using fluorescent reporters, i.e. QDs, organic dyes and autofluorescent proteins, which deliver a limited photon budget before they photodissociate. The highest localization accuracies and the best temporal resolutions require a large number of photons, reducing therefore the observation time in the case of fluorescent reporters. Although non-fluorescence reporters outperform in terms of optical properties compared to fluorescent emitters, their large size might adversely influence the biological system so that in practice a compromise should be established regarding the phenomenon under study and the reporter to be used. The next section focuses on these aspects.

2.2. Probe reporters and their importance for SPT

A crucial part of SPT is the actual reporter to be tracked, also known as the probe. In general, the biomolecule of interest must be first labeled with a reporter in order to be detected optically. Since direct labeling is not normally possible, the attachment of the reporter to the biomolecule is performed using specific biochemical strategies. An exceptional case is autofluorescence proteins, where the protein of interest is genetically modified to become fluorescent and can be directly tracked [54]. Following the terminology of Clausen & Lagerholm, a SPT probe consists then of two parts: a 'specificity' module which renders specificity to the biomolecule; and a 'label' module which gives indirect visualization of the target biomolecule, being the one to be followed optically [55]. Figure 2 shows some of the most common molecules used for providing specificity as well as the optical labels. Specificity modules include full antibodies, single chains, Fab fragments, streptavidin, nanobodies or specific epitope tags introduced first in the target molecule in order to confer labeling specificity. For detailed information on different specificity modules the reader is referred to excellent recent reviews on the topic [30, 31, 44, 55].

Both the physico-chemical and the optical properties of the probe have an enormous influence on the quality of the SPT data, and they have to be carefully chosen according to the biological process being investigated. Unfortunately, these properties oppose each other. From the physico-chemical point of view, the probe should be highly specific to the biomolecule, ideally in a 1 : 1 binding ratio, and should not influence the biomolecule's mobility or ability to interact with its environment [55]. To meet these requirements, the smallest probes are preferred, i.e. the smallest specificity module and the smallest label module. From the optical point of view, the probe should be very bright, i.e. having a large absorption cross-section and high quantum yield in the case of fluorescent emitters, or a large scattering cross-section in the case of non-fluorescent reporters. These properties are important to provide high temporal resolution and spatial localization accuracies. In addition, the probe should be highly photostable (low photobleaching rate) to allow for long observation times. Physically larger reporters, and in particular gold nanoparticles, meet these requirements. It is worth mentioning that in the search for smaller but brighter and more photostable probes, new SPT techniques are currently being developed allowing the detection and tracking of metal particles as small as 5 nm in diameter. The principles of these techniques are described in section 2.3.4.

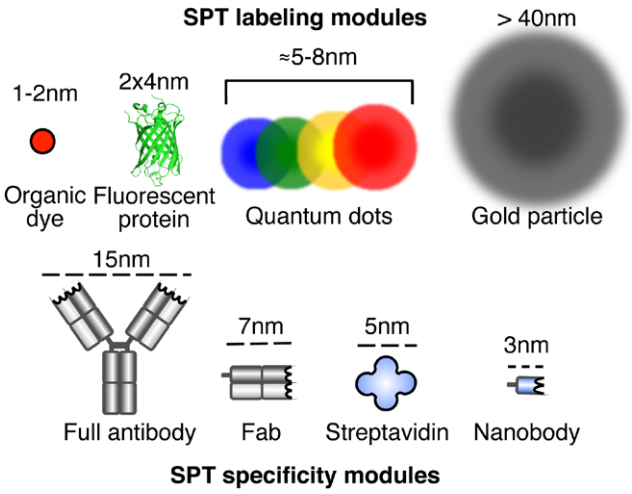

Figure 2. Common reporters used in SPT. Labeling modules include organic dyes, fluorescent proteins, QDs and gold colloid particles. The approximate size of these different labels is given in the picture. In the case of QDs, the sizes correspond to inorganic CdZe QDs prior to the biofunctionalization step. Specificity modules allow the attachment of the label probe to the biomolecule of interest. They include specific antibodies, Fab fragments, streptavidin and nanobodies (antibody fragment consisting of a single monomeric variable antibody domain). Their approximate size is given in the picture.

Gold particles 40 nm in diameter have the best optical performance for SPT, but they might reduce the mobility of the biomolecule under study, induce cross-linking with other biomolecules and/or affect the biomolecule's interaction with the environment [38, 55]. Moreover, since the detected signal is based on light scattering, gold particles do not allow for multicolor experiments, which is one of the main advantages when using fluorescent probes.

On the other hand, extreme organic fluorescent dyes are the smallest possible SPT labels (between 1–2 nm in diameter). They are extremely versatile, i.e. they can be used for tagging lipids, proteins, DNA, etc; and they can be used in combination with a large variety of specificity modules using well-established bio-conjugation protocols [56]. Their small size

also guarantees minimal perturbation of the bio-functionality of the molecule under study. The main disadvantage of fluorescent dyes is their poor photostability and small absorption cross-section, restricting their imaging to only a few seconds with somewhat poor localization precision and temporal resolution. Although photobleaching can be reduced by the use of specific scavengers that remove free oxygen, their use poses a serious obstacle to many experiments in living cells due to the toxicity of oxygen scavengers [57]. Multi-color SPT with organic dyes is readily possible [58, 59], albeit their broad emission spectra limits in practice the number of different spectrally separated dyes to two or three at most.

Autofluorescent proteins are slightly larger than organic dyes but have the major advantage of being genetically encoded to the biomolecule of interest, avoiding the chemical modification of the biomolecule or the addition of a specificity module. They are particularly useful for the investigation of intracellular processes, as the proteins are directly generated through the natural protein expression pathways [54]. Like organic dyes, autofluorescent proteins exist in a wide range of colors and modified forms to allow for calcium sensing or being photo-switchable or photo-convertible [60, 61]. Unfortunately, they perform even worse than conventional organic dyes in terms of optical properties, with broader emission spectra, lower quantum yield and extinction coefficients, and a lower number of emitted photons before photodissociation. Moreover, their emission is highly intermittent (i.e. they show on-off-blinking) already at low excitation powers [62], making SPT in living cells highly challenging.

QDs provide nowadays the best compromise between size and optical properties and as such are being increasingly used for SPT. QDs are semiconductor nanocrystals whose emission wavelength can be tuned by the size of the nanocrystal (due to quantum confined effects [63, 64]). Their inorganic cores (from where the luminescence is emitted) range from 4 to 10 nm in diameter, but their necessary stabilization and functionalization to make them biocompatible require additional layers resulting in a final diameter between 10–30 nm [31, 44, 65]. While these sizes are lower than gold colloids, they might still perturb the bio-functionality of the labeled molecule. Moreover, although their functionalization can be easily performed using standard bio-conjugation procedures (reviewed in [31]), controlling the valency of functionalized QDs is still challenging (i.e. the number of binding sites on the functionalized outer layer of the QD). Because of this polyvalency, multiple target molecules can attach to the same QD potentially inducing cross-linking of the target molecule. This in turn will bias the observed mobility, could trigger internalization of the membrane targets or unwanted signaling cascades (reviewed in [31]). Driven by their excellent optical properties numerous strategies are currently under development to reduce the overall size of QDs and to make them monovalent using new surface coatings and bio-conjugation strategies (for insight into recent developments see [31, 66]). Their use for monitoring intracellular processes is still rather limited given the current difficulty in delivering them inside the cell [31, 65], so many of the QD-SPT applications focus on studies of membrane dynamics and organization (see section 4). From the optical side, QDs are far superior to organic dyes and autofluorescent proteins. They are extremely bright due to their large extinction coefficient, which is at least ten times larger than the best dyes [63–65], allowing precise localization within a few nanometers and reducing integration times, leading to increased temporal resolution (a few milliseconds). Importantly, they are highly photostable [63], providing 2–4 orders of magnitude more photons before photodissociation than organic dyes. This enables the study of QD-labeled molecules for extended durations (typically tens of minutes). Moreover, their broad absorption and narrow, symmetric emission spectra (typically 30–50 nm broad) enable single wavelength excitation and truly multi-color imaging with little spectral cross-talk [67, 68]. One of the major optical drawbacks of QDs is their power-law on-off intermittent emitting behavior [69–71], i.e. the alternation between bright and dark levels of intensity, also known as blinking. This effect causes major problems when trying to reconnect the centroid positions to generate long QD trajectories. Different strategies have been developed to both chemically reduce the blinking behavior of QDs [72, 73] as well as specific algorithms to minimize its effect while reconnecting trajectories [74].

2.3. Optical implementations for 2D and 3D SPT

2.3.1. SPT in 2D. The most commonly used (and easiest) SPT optical implementation for 2D imaging relies on wide-field illumination and detection using a low-noise, highly sensitive camera. This configuration allows for the parallel detection of multiple reporters, providing rapid data acquisition for tracking moving molecules. Since nowadays most of the SPT studies use fluorescent reporters we are restricted here to the implementation of optical set-ups based on single emitter fluorescence excitation and detection (see figure 3(a)). Usually the reporter is excited using a laser beam focused on the back focal plane of the objective to create a parallel beam that excites a region of the sample throughout its entire depth. The emitted fluorescence is filtered out from the excitation light and detected using a camera. The detection and tracking of individual emitters requires high signal-to-background ratios, which depend on the photophysical properties of the probe used (described in the previous section), the surrounding background and the fluorescence collection efficiency of the set-up. Typically, objectives with NA > 1.2 are used to collect the largest possible number of emitted photons. Moreover, sharp fluorescence filters with high transmission (>80%) and camera detectors with high quantum yields and fast frame transfer are preferred. Modern electron-multiplied charge couple device (EMCCD) cameras make use of on-chip electron amplification before read-out providing fast continuous read-out at high quantum yield and optimum resolution [75]. For dual-color imaging, the spectrally separated fluorescent signals can be sent to different portions of a single camera or to separate cameras. Different cameras have the advantage of an increased field of view and the use of different frame rates per color channel, but are more difficult to align and increase the cost of the set-up.

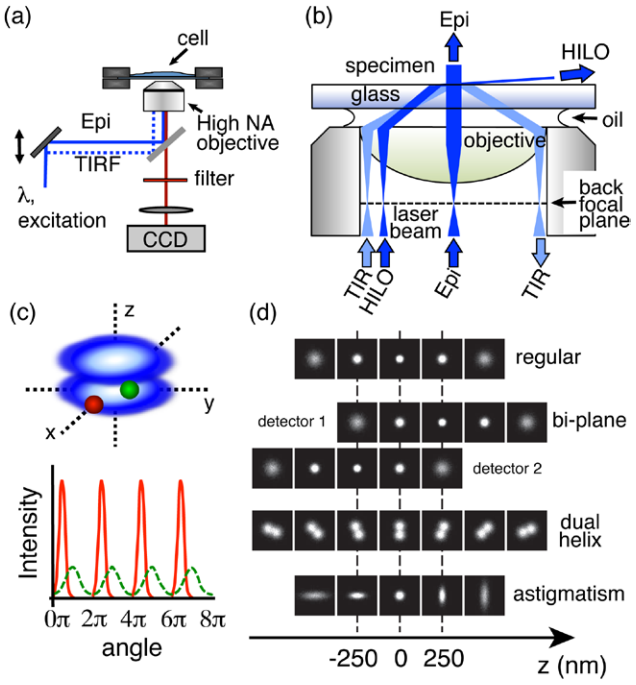

Figure 3. Different optical schemes for SPT in 2D and 3D. (a) In its simplest implementation a laser light is coupled into a high NA objective either in epi or TIRF mode. The emission light is separated from the excitation light using suitable filters and detected using a CCD camera. This configuration can be easily adapted to include multiple excitation lasers that can be selected or temporally alternated using an acoustic-optical tunable filter. The detection path can be modified to include several cameras or by sending the detected light (spectrally separated) to different regions of the same camera. (b) Different illumination schemes, including epi, TIRF and HILO. In these configurations, the laser beam is focused on the back focal plane of the objective. Depending on the inclination of the laser beam with respect to objective axis, different illumination depths are achieved. (c) Principle of orbital tracking of particles in 3D using two-photon microscopy. The laser is scanned in circles surrounding the particle of interest (blue ellipses). In the example, two orbits at different z-positions and two different particles (green and red) are shown. The fluorescence intensity is integrated at given points of these orbits as the laser moves around the particle. The intensity is related to the actual position of the particle with respect to the orbit and used to track the position of the particle in 3D. (d) PSF engineering approaches that break the axial symmetry of the regular PSF to encode 3D information in the PSF shape.

In live cell experiments, most of the associated background arises from cell autofluorescence, so that one obvious way to minimize background is to reduce the illumination volume. Depending on the cellular region to be investigated, i.e. cell membrane and intracellular or nuclear compartments, several optical schemes have been devised to reduce the background contribution from cell autofluorescence. For cell membrane studies the most favorable illumination scheme is based on total internal reflection fluorescence (TIRF) excitation, whereas highly inclined illumination [76] or light sheet illumination [34, 77, 78] are more suitable for tracking inside the cell or even in tissues (figure 3(b)). In the case of TIRF, an evanescent field is generated at the glass–water interface by total reflection of the excitation laser. Because the evanescent field decays exponentially along the axial direction, the extent of illumination is limited to ~200 nm away from the interface, avoiding excitation of unwanted fluorescent components within the cell interior (reviewed in [79, 80]). Nowadays, most common SPT set-ups achieve TIRF excitation by means of a high NA objective (see figures 3(a) and (b)), allowing easy exchange from wide-field to TIRF (or inclined illumination) and back, depending on the sample conditions, increasing the flexibility of the instrument. TIRF provides excellent signal-to-background ratios and it is particularly powerful for cell membrane studies, since the basal cell membrane is normally in contact with the glass surface. This great advantage is also the main limitation of the technique, as only the basal cell surface and the nearby cytoplasmic zones beneath the plasma membrane can be excited.

To visualize different regions of the cell interior, highly inclined and laminated optical (HILO) sheet illumination can be implemented [76]. Instead of reaching total internal reflection, the incident laser beam is highly inclined by a large refraction and is laminated as a thin optical sheet at the specimen side (figure 3(b)). The background is reduced since only a thin layer of the cell interior is illuminated, but it only works in a limited depth range and in the center of the object field. At the edges of the object field, the inclined beam illuminates the sections below and above the focal plane, respectively, resulting in image blur and loss of contrast. A significant improvement over HILO is provided by light sheet illumination [81]. In light sheet fluorescence microscopy (LSFM), the illumination and detection light paths are separated geometrically. Optical sectioning is achieved by illuminating the specimen from the side using a thin sheet of light (a few micrometers thick). Although the method has been mostly applied as a 3D imaging technique for studies in transparent multi-cellular organisms or chemically clear tissue [82–84], the improved signal-to-background ratios brought about by optical sectioning have recently allowed the single-molecule imaging of transcription factor binding to DNA in live mammalian cells [34].

A different optical configuration that reduces the background is confocal excitation of the sample in combination with a single point detector, such as a photo-multiplier tube or an avalanche photodiode detector. Although this method rejects out-of-focus light, increasing significantly the signal-to-background ratios, the reconstruction of an image requires the scanning of the sample or the excitation laser, reducing acquisition rates (less than 10 frames s^{-1}) and restricting this approach to the study of very slow dynamic processes. With the use of spinning-disk confocal microscopy, the image acquisition rate can be increased by typically one order of magnitude, being particularly useful for tracking dynamic processes inside cells [85–87].

As briefly mentioned in section 2.1, the experimental conditions of SPT impose the use of sparse labeling since particle localization requires that the molecular separations at any given time of the image recording are larger than the particle's diffraction-limited size. This limitation results in practice in a spatiotemporal compromise in any given SPT experiment. Several strategies are currently being developed to increase the labeling density. One approach relies on an algorithm that uses recursive fitting of the highest-intensity centroid

positions, followed by a deflation loop that subtracts detected peaks and allows detection of additional peaks that were previously masked because of their lower intensity [74]. In this way, densities of up to one molecule per μm^2 can be reliably handled. A different approach combines photoactivated localization microscopy (PALM) with SPT (called sptPALM) [88]. The method consists of activating, localizing and bleaching many subsets of photoactivatable fluorescence-proteins. Using time resolutions of 50 ms frame^{-1} Manley *et al* demonstrated individual tracking of photoactivated molecules on the membrane of living cells appearing during the course of hundreds of seconds (each trajectory lasting for less than 1 s). In addition, the very high density of the total tracked proteins (50 per μm^2) enables the creation of spatial maps of diffusion coefficients, accounting for the heterogeneity of molecular environments within cell compartments [88–90]. In addition, sptPALM benefits from the large palette of different autofluorescent proteins available nowadays [61] and can be used for monitoring cell membranes as well as intracellular processes. The current limitations of sptPALM are the poor photophysical properties of autofluorescent proteins, yielding very short trajectories and poorer positional precision. Furthermore, high transfection levels of autofluorescent proteins are required, interfering with the endogenous protein population (the level of protein expression that a cell will normally produce).

A related method is based on continuously and stochastically labeling a low number of biomolecules with fluorescent ligands in solution while imaging the sample with oblique illumination (known as universal points-accumulation-for-imaging-in-nanoscale-topography, uPAINT) [91]. This method uses a low concentration of fluorescent ligands introduced in the extracellular medium such that a low constant rate of molecules on the cell surface is labeled during the imaging sequence. The oblique illumination of the sample is used to excite predominantly fluorescent ligands that have bound to the cell surface while not illuminating the molecules in the above solution. Because the method uses conventional organic dyes, trajectories longer than those obtained with sptPALM can be recorded (tens of seconds) with molecular densities as high as 120 μm^{-2}. Importantly from the biological point of view is the fact that in uPAINT, the endogenous population of proteins are labeled and imaged, but unfortunately so far, the method is restricted to extracellular binding on live cells. Other related novel methods include the use of stochastically active organic dyes using specific tags (SNAP or HALO) to label intracellular components and to achieve high density SPT in intracellular compartments [92, 93]. In principle, any of the methods described above can be also combined with multi-color imaging to further increase the density of the recorded trajectories (describe in more detail in section 2.3.3).

2.3.2. SPT in 3D. Tracking molecular events in 3D is notably more challenging that 2D-SPT, but highly powerful to extend SPT experiments to intracellular or nuclear compartments, and even to multicellular systems. Therefore, much effort nowadays is focused on the implementation of optical set-ups, labeling strategies and dedicated data algorithms for tracking the motion of individual particles in 3D. A number of optical approaches have been explored in the last few years, some of them summarized in figures 3(c) and (d). The initial methods developed for 3D-SPT used confocal microscopy to record a series of (confocal) image stacks in the z-direction [36, 81, 94] together with deconvolution algorithms to locate the particle of interest with high precision. However, the slowness of the method restricts the number of applications to extremely slow dynamic processes. Although spinning-disk confocal microscopy provides much higher temporal resolution [85], it does not provide, in general, sufficient sensitivity for the detection of individual fluorescent molecules. A more elegant method (using two-photon excitation) implemented by the Gratton group uses a clever orbital scanning scheme together with a feedback loop to track the particle as it moves in 3D [95, 96]. The temporal resolution is improved because the confocal volume is not scanned across the sample to generate images, but rather it moves in circular orbits around the particle of interest (figure 3(c)). Using this scheme, single particles can be located with a precision of 20 nm in 16 ms when tracking in 2D, and 32 ms when tracking in 3D [95, 97]. The general disadvantage of this method is that only a single particle is tracked at one time, so collecting enough statistical data is cumbersome.

Because of its simplicity, wide-field combined with tailored ways of illumination, including HILO and light sheet, have been implemented for tracking in 3D. The most straightforward approach takes advantage of the size and shape of the intensity spot (the PSF of the microscope) when is de-focused to infer on the z-position of the particle (figure 3(d)). As already mentioned in section 2.1, at the focal plane, the PSF basically consists of the main Airy disk. As the particle moves away from the focal plane, the size of the PSF increases and, for large z-displacements from the focus, ring intensity patterns are formed. By measuring the radius of the outermost ring the actual z-position of the particle can be determined [98]. This approach can be used to follow particles moving within a range of 3 μm from the focal plane, depending on the intensity of the particle, although the precision in the radial position decreases with the distance from the focal plane since the intensity patterns become weaker. Moreover, the absolute z-position (above or below the focal plane) cannot be unambiguously determined. Alternative approaches that rely on the shape of the PSF of the microscope use a multi-focal plane to increase the localization precision in the axial direction [99, 100] or a phase element to engineer the PSF with the shape of a double helix [101]. This latter method provides nearly constant localization over an axial range of up to 2 μm, but it is limited by the low transmission efficiency of the phase element used to shape the PSF. Another defocusing method introduces a cylindrical lens in the detection path to generate axial astigmatism in the collected image [102, 103]. At the focal plane the PSF is circular, but above and below the focal plane the PSF becomes ellipsoidal, with the major axis of the ellipsoid shifting by 90° while going through the focus. Since the amount of astigmatism and thus the exact shape of the PSF strongly depends upon the z-position, the absolute z-position of the particle can be determined from the size and the orientation of the ellipsoid. High z-accuracies (between 10–30 nm)

within 1 μm of the focal plane have been reported using this approach [102].

2.3.3. Multi-color SPT. Multi-color SPT is a powerful tool to track and quantify interactions between the same species or between multiple components. In the case of two-color SPT, spatially overlapping particles can be separated by their emission spectra using suitable filters. However, extending the detection to more than two colors is challenging given the spectral overlap between different fluorophores or fluorescence proteins. This can be particularly problematic due to the broad spectral emission of autofluorescent proteins, or when the labeling ratios between different components are very large. Several strategies have been implemented to overcome or at least reduce the severity of spectral crosstalk: alternating different lasers on the excitation side, or by the use of QDs, which have very narrow emission spectra. In the first case, the removal of spectral cross-talk is achieved by collecting consecutive frames using alternating excitation wavelengths [59, 104]. With an appropriate choice of excitation wavelengths and fluorescent filters, the high-energy fluorophores will be not be excited with the lower energy wavelengths. This method is particularly suitable when using autofluorescent proteins for intracellular applications, but the complexity of the set-up increases when extending this approach to more than two colors.

QDs are particularly suitable for multi-color experiments, given their narrow and symmetric emission spectra. In addition, they have a broad-band absorption, which simplifies the excitation path of the set-up, as only a single laser (typically at $\lambda = 488$ nm) can be used to simultaneously excite multiple QDs. Dual-color QDs have been applied to many different studies on cell membranes by sending the spectrally separated fluorescent signals to two different parts of the same CCD camera (reviewed by [31]). Extending to four colors can be achieved using a single [66] or two spectrally separated cameras. A new powerful method, called high-speed hyperspectral microscopy (HSM) has been recently implemented to perform SPT of up to eight spectrally distinct species of QDs with frames rates below 40 ms [68]. In HSM, a single laser excitation ($\lambda = 488$ nm) is focused on a line providing high excitation intensity to a small volume of diffraction-limited width. After blocking the excitation light, the collected signal is sent to a spectrometer, which distributes the light onto an EMCCD camera such that each exposure captures information on wavelength and position along the line. To generate a 2D hyperspectral image, the excitation line is then scanned across the sample plane in discrete steps. The current limitations of this technique are given by the readout rate of the EMCCD, but with the continuous development of faster, more sensitive and low pixel-to-pixel noise of the newest cameras, higher acquisitions rates could be expected in the near future.

2.3.4. Non-fluorescence-based novel SPT approaches. All of the optical implementations described above rely on the efficient detection of fluorescence as the basis for SPT. Despite the many advantages of using single fluorescent emitters as SPT reporters, their intensity and duration of their emission imposes fundamental limits on the imaging speed and precision for tracking studies. Although QDs are considerably more stable than conventional dyes and autofluorescent proteins, their somewhat large size can still interfere with the biological process under investigation. Therefore, novel techniques based on contrast mechanisms other than fluorescence are currently being developed to allow the detection of small non-fluorescent reporters for SPT applications. One such a technique is based on photothermal heterodyne imaging of small gold nanoparticles, down to 1.4 nm in diameter [105, 106]. This technique takes advantage of the efficient light absorption of metallic particles and the fact that almost all of the absorbed energy is converted to heat. The increase in temperature induced by absorption gives rise to a local variation of the local refractive index around the nanoparticle, which can be monitored using specific instrumentation combining heating and probe laser beams. To increase the sensitivity of the method, the heating beam is modulated, inducing a time-modulated variation of the refractive index around the absorbing nanoparticle. The interaction of the probe beam with the time-modulated signal produces a scattered field with sidebands at the modulation frequency. The forward scattered field is then detected using a photodiode coupled to a lock-in amplifier. Imaging is performed by moving the sample over the fixed laser spot by using a piezo-scanner. SPT is achieved by means of a triangulation algorithm over a small region of the sample, i.e. measuring the signal at three well-defined positions around the tentative location of a nanoparticle as a function of time [107]. Using 5 nm-gold particles, positional accuracies of 20 nm at tracking rates of 30 Hz for extended observation times (several minutes) have been demonstrated on living cell membranes [107], and more recently inside cells [108]. Currently, this method requires extremely high excitation intensities to obtain high signal-to-noise ratios (SNRs), which can be detrimental to the cell. Moreover, since the acquisition of the trajectories is serial, the collection of statistical data becomes quite tedious.

Interferometric scattering microscopy (iSCAT) is another powerful non-fluorescent based approach that relies on the interference of the light created by Rayleigh scattering and the reflection of the incident laser beam at the substrate-water interface [39]. This technique is able to detect relatively small metal nanoparticles, or large individual biomolecules without the need for external labeling [109, 110]. In iSCAT a laser beam illuminates a glass substrate and its partial reflection at the glass interface is used as a reference for homodyne interferometric detection. Molecules on the glass surface will scatter light that is collected with an objective. Both the reference beam and the scattered signals are sent to a CMOS camera. Because the two fields are coherent they will interfere, resulting in an interference term that is proportional to the scattering power and to the power of the reflected beam. Thus, the interference term to be detected (containing the signal of the scatterer) can be amplified by increasing the incident beam power. A major complication of this technique is the associated background, not only from fluctuations in the laser power, but importantly, from additional background scattering

of surrounding objects or substrate roughness that makes it difficult to identify the signal of interest and reduces the effective SNR. With extremely well-controlled experimental conditions, 20 nm gold particles have been successfully tracked on artificial membranes with 2 nm localization precision and 20 μs temporal resolution [111]. Individual (large) unlabeled biomolecules have also been recently detected using this approach [110, 112]. Unfortunately, since living cells are highly scattering structures, it is difficult to foresee how this approach could be implemented to track small nanoparticles or unlabeled biomolecules on biological cell membranes or inside living cells. Nevertheless, given the remarkable superiority of small gold nanoparticles in terms of photostability, size and easy coupling biochemistry, we predict that further developments in photothermal imaging, iSCAT or even newer optical configurations will continue in the next few years.

3. Data analysis

The general output of a SPT experiment consists of a time-series of diffraction-limited images of particles obtained via microscopy-based techniques. A crucial step for the quantitative assessment of the dynamic properties is the detection with subdiffraction resolution of each particle position and their connection in order to reconstruct single-particle trajectories (figure 1). This process, often ambiguously referred to as 'single-particle tracking' as well as the whole technique [21], was first performed manually or in a user-assisted fashion [30]. Besides being tedious and time-consuming, the need for high-throughput data requires a high number and density of particles, therefore several advanced computer algorithms have been developed to achieve precise and accurate localization (reviewed in [113, 114]) and unbiased tracking (reviewed in [21, 30]).

Once the trajectories are obtained, further analysis must be performed in order to interpret and classify the dynamics of the system. Typically, this is achieved by the calculation of the mean-square displacement curves and their fitting to models corresponding to different types of motions (e.g. pure diffusion, anomalous subdiffusion, confined motion, immobile and directed motion). Classification of the type of motion and quantifications of dynamic parameters is not always straightforward due to the positional error and poor statistics in short trajectories. In addition, particles can display transitions between different types of motion within the same trajectory or space-dependent dynamics, whose quantification requires dedicated tools for their detection and analysis.

3.1. Algorithms for particle localization

The raw data of SPT experiments typically consists of a time-sequence of diffraction-limited images of fluorescent particles. In each frame of a sequence, particles appear as blurred spots over a noisy background. The intensity profile associated with a particle is given by the convolution of the particle shape with the PSF, i.e. the transfer function of the imaging system. The PSF width, proportional to the ratio between the fluorescence emission wavelength and the numerical aperture of the imaging lens, determines the spatial resolution of the microscope, whereas the PSF intensity is proportional to the expected number of collected photons.

The first step in SPT analysis consists of particle localization: the bright spots corresponding to fluorescent particles must be separated from the background and their centroid coordinates determined with sub-pixel precision. This task is crucial for the ensuing SPT quantification, since errors in the localization might induce artifacts and limitations in the determination of particle dynamics. In addition, exhaustive and reliable particle detection is required in order to obtain long trajectories and high-throughput data, while preventing false-positive assignment of localizations to noise-related features. Once the particles have been localized, the following step involves 'connecting the dots' [115], i.e. associating the localizations from frame to frame in order to construct a trajectory. At ultra-low particle densities, this connection corresponds to simply joining the nearest dots from frame to frame. As the density is increased, connecting the trajectories becomes an intense combinatorial problem as ambiguities can arise from path-crossing and particle appearance/disappearance, either due to fluorophore photophysics or to false-positive and missed localization. Limited or wrong reconnection of localizations can impact the data by either producing short, fragmented trajectories or wrongly joining localizations belonging to different particles.

Many potential artifacts associated with the extraction of single-particle trajectories from raw data can be reduced experimentally, by the use of bright and stable probes, relatively low particle densities, sensitive low-noise detectors, high collection efficiency and high SNR. However, dedicated analytical approaches are required for obtaining unbiased detection while at the same time allowing fast and automatic data processing. Due to the huge spreading of SPT, a large number of complex algorithms have been developed, involving advanced tools from signal analysis, computer vision and statistics. A recent community experiment was performed to evaluate the performance of 14 different tracking algorithms in distinct simulated experimental scenarios [21]. The evaluation resulted in no clear winner, but gave interesting hints for the selection of the most appropriate method for each given condition [21, 116]. Describing the details of all the proposed methods goes beyond the scope of this review. Nevertheless, in the following we will briefly outline the general approach used by these algorithms, and explain in some detail their common aspects.

The first task is to estimate the centroid coordinates of the fluorescence spots, thus locating the particle from its digitized image with sub-pixel precision (figures 4(a)–(d)). Determining the location of a particle from its image is not straightforward. Both the emission and detection of photons are stochastic processes for which the PSF only predicts the average number of counts. The presence of background and shot-noise hides dim features and limits their detection. Moreover, as there is no ideal noise-free detector, the data are further corrupted by pixelation and readout-noise [113]. As a result of these factors, the location of a fluorescent particle cannot be precisely

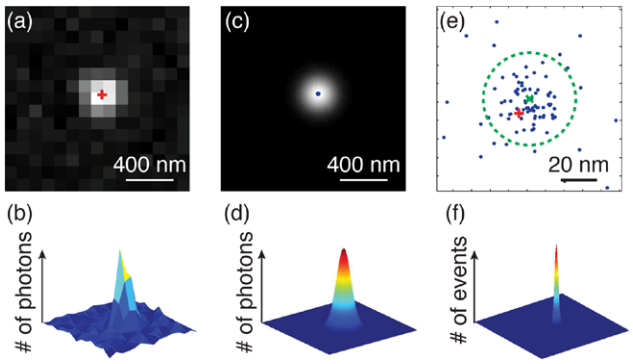

Figure 4. Estimation of particle centroid position and calculation of localization precision. (a), (b) Simulated diffraction-limited image of an isotropic fluorescent emitter, including the effect of Poisson noise and detector pixelation (a), and corresponding photon counts histogram (b). The red symbol in (a) represents the actual position of the emitter. (c), (d) Results of a weighted least-square fit to the data in (a), (b) by means of a 2D Gaussian function. The estimated centroid position is shown as a blue dot in (c). (e), (f) Position estimates from different images of the same emitter (blue dots). The green cross corresponds to the average of the individual localizations, whereas the green circle denotes their standard deviation, corresponding to the localization precision. The difference between the average localization (green cross) and the actual particle position (red symbol) gives the localization accuracy. The probability distribution of individual localizations (f) is represented on the same scale as (b) and (d).

determined from its image, but only estimated with a certain error [114, 117–119] (figures 4(e) and (f)). This error can be quantified by means of the localization precision and accuracy. The localization precision refers to the standard deviation of the estimation of the particle's actual position around its mean. It must not be confused with the localization accuracy, which refers to the deviation of the mean estimated position from the actual position [114] (figure 4(e)).

Another factor to take into account is that particles continuously move during the image acquisition. Therefore, the distance traveled by a particle during the acquisition time produces a change in the shape of the PSF [120] and an inherent decrease in localization precision [121].

Due to the large spread of SPT and of other fluorescence techniques based on particle localization [122–124], several methods have been developed for localizing particles from diffraction-limited images, attempting to achieve the highest localization precision. The variety of localization methods reflects the large number of configurations available for SPT, including different fluorescent probes, setup designs and detection schemes (see section 2). This abundance challenges a rational and exhaustive classification of all the proposed methods. Nevertheless, a major classification can be made based on fitting and non-fitting methods. Fitting methods retrieve the particle position by fitting the image by means of a suitable model function and are probably the most rigorous and most widely used approaches. The fitting function must be properly chosen based on the properties of the fluorescent probe in order to be a valid model for the data. For small particles, assumable to point-like emitters, such as single molecules, small beads or QDs, the fitting function is essentially given by the PSF of the optical system. A circularly symmetric PSF is a valid assumption for isotropic particles, i.e. if the signal is averaged over many orientations of the emitter's dipole, because the emitter rotates faster than the imaging rate. For point-like anisotropic emitters, the image is instead affected by the dipole orientation [125]. In these cases, fitting methods can still be applied provided that a suitable model function is available [126–129]. Fitting methods can also be used for larger particles, having one or more dimensions of the order of the optical resolution, or for particles labeled with multiple fluorophores. In the latter case, emitter dipole orientation is not an issue since the emitters will have different orientations and the model function must approximate the convolution of the object shape with the instrumental PSF [114]. Fitting models are also applicable to 3D tracking, although with different approaches depending on whether the image is obtained by single-plane or confocal imaging. In the first case, information about the axial dimension is obtained by measuring changes in the width, shape or orientation of the PSF (in addition to its center in the 2D image), as do analysis techniques for dipoles [114]. In the case where the 3D imaging is performed by multi-plane confocal scanning, the image is fitted to a 3D PSF model, such as an anisotropic Gaussian function [130]. In all the cases, a misspecified PSF or model function can cause systematic biases in shape estimation and, thus, imprecision in the determination of the particle coordinates. Other factors that can affect the localization are the source and modeling of noise, and the optimization method. The details of these approaches have been recently extensively reviewed [21, 113, 114]. In the following, we will briefly discuss the localization precision and limitations induced by these factors for the localization of isotropic point-like particles in 2D. Although some of the conclusions are rather general, we refer the reader to these works for an extended discussion of the other cases [21, 113, 114].

For small isotropic point-like particles, such as fluorophores or QDs, fitting-based approaches require (at least) an approximate knowledge of the shape of the PSF. The choice of an accurate PSF is important, since its misspecification affects localization precision [118], but generally does not introduce bias if the actual PSF is approximately symmetric [131]. Numerous geometrical and optical factors affect the shape of the PSF. Highly accurate PSFs can be obtained by means of sophisticated models [132, 133]. However, in the isotropic and aberration-free case, the typical PSF pattern is a central spot whose width corresponds roughly to the wavelength of light and then the Airy function is a valid approximation at low numerical apertures [118, 119]. However, for many practical cases, the PSF of an isotropic source can be approximated with a Gaussian function [134], allowing simpler mathematical calculations. Other important characteristics of the fitting methods are the parameters used to minimize the mismatch between the data and model. Besides particle coordinates, the fitting model can also include an estimation of peak intensity and noise [113]. The background noise is a key variable and its correction is fundamental to obtaining unbiased results [118]. However, accurately accounting for the noise in a SPT experiment is complicated by the presence of several

sources of error, either generated by detectors (shot-noise, read-out noise, electron multiplication process in EMCCD, or pixel-dependent noise in sCMOS cameras) [135–137], or by the sample preparation (spurious fluorescence, out-of-focus particles, cell autofluorescence) [114]. Therefore, when a suitable approximation of noise model is not available, care should be taken in the choice of the algorithm and it might be preferable to use methods that can handle limited information [113]. Parameter optimization can be performed either by means of nonlinear (un)weighted least-square minimization [138] or maximum likelihood estimation [118]. The localization precision achieved by these fitting approaches has been widely studied [117–119]. In the shot-noise-limited case, the variance associated with particle localization simply scales as the inverse of the number of collected photons [117]. When including other sources of error, such as the background noise (e.g. arising from readout error or spurious fluorescence) and the indetermination in photon arrival position introduced by the finite pixel size, an approximated formula for the calculation of localization precision was proposed by Thompson *et al* [117] for the least-square fitting to a 2D Gaussian function. More generally, a fundamental limit to the achievable precision might be calculated, independently on the fitting model, by the Cramer–Rao lower bound (CRLB) [118, 119]. It has been shown that the maximum likelihood estimation provides better results as compared to the least-square fitting at low photon counts and can get closer to the maximum precision predicted by the CRLB [118, 139, 140].

In spite of the excellent results achievable by means of fitting approaches, no theorem or principle precludes an estimator from obtaining localization close to the CRLB [113]. Therefore, several non-fitting methods have been proposed and constitute a valid alternative to fitting when computational speed and simplicity are required, while achieving precision and wide applicability. In addition, the limited number of assumptions about image shape makes them advantageous for tracking diffusing emitters [120, 121]. Non-fitting methods have been devised based on several different strategies, ranging from simple intensity-based centroid calculation [141, 142], triangulation [143, 144] or the phase shift of the Fourier transform [145]. While these methods are fully model-independent, others use the knowledge of PSF properties, such as its radial symmetry [131].

Both fitting and non-fitting methods are often included in more refined algorithms, which can combine preprocessing to reduce noise, the selective enhancement of objects by filtering (using median, wavelet-based, Gaussian, Laplacian-of-Gaussian or other filters), routines for the identification of prominent spots (often using local-maxima finding and/or thresholding) as well as iterative localization procedures to obtain better precision [21, 146–156].

Recently, significant efforts have been devoted to the development of localization algorithms capable of estimating positions of overlapping emitters in high-density images [74, 135, 157–162]. Although most of these methods were originally designed for super-resolution microscopy with the aim of improving the acquisition speed, the capability of resolving closely spaced objects also has utility in SPT [68, 74], since it results in higher data throughput. These algorithms consist of the fit of a multiple emitter model (i.e. a sum of PSFs or model functions) and, similar to other fitting methods, can be implemented via both least-square minimization or maximum likelihood estimation. Crucial parameters of these methods are the false-positive and the missed-localization rates, since they tend to favor models with larger numbers of emitters. Therefore, a threshold criterion must be carefully defined in order to decide when to stop adding localizations without impacting the missed localization rate.

3.2. Algorithms for particle linking

Once the particles coordinates are found, a linking algorithm is needed to connect the particle localizations frame-by-frame in order to construct the trajectories (figure 5). In the simple case of low emitter densities, this task can be performed in an automatic fashion by sequentially joining the localization by means of a separation-based criterion, such as the nearest-neighbor distance (figure 5(a)). For each particle localized in a given frame, the distances with all the localizations obtained in the next frame are calculated. The pairs of localizations showing the minimum distance are selected as the most likely occurrence of the same particle in successive frames and are linked together. Repeating this procedure over all the particles and all the frames finally provides the reconstructed trajectories. However, experimental conditions often prevent this scheme from working reliably (figure 5(b)). A first challenge is posed by the possibility that particles permanently or temporarily disappear due to blinking, photobleaching or missed localization. The criteria for stopping a trajectory reconstruction when no localizations are found within a given distance must be included. For similar reasons, a particle can (re)appear at any given frame during the recording. Therefore, the linking process must deal with these events and be capable of closing gaps originated from blinking particles and/or missing localizations. At high densities, the complexity is further increased by the possibility of particles crossing each other and ambiguities can arise when joining the localizations. In order to account for these problems, algorithms have been developed in order to use the largest set of information and to provide reliable tracking. Many approaches include multi-particle tracking, i.e. all the trajectories are simultaneously reconstructed and an optimization strategy is used to resolve conflicts between competing assignments. Moreover, accumulated evidence from multiple frames can also be used to improve tracking. In this case, trajectory reconnection can be generally treated as a combinatorial optimization problem with a factorial complexity and it is therefore a non-deterministic polynomial-time hard problem [163]. A cost function or metric, including all reconnection possibilities, must be built and minimized. However, for this class of problems, finding a global solution without approximations is computationally unfeasible even for tens of particles [164]. To circumvent this constraint, tracking algorithms solve particle correspondence locally. Several schemes have been developed going beyond straightforward nearest-neighbor linking and using sophisticated tools from statistics, signal analysis and computer vision [74, 130, 146,

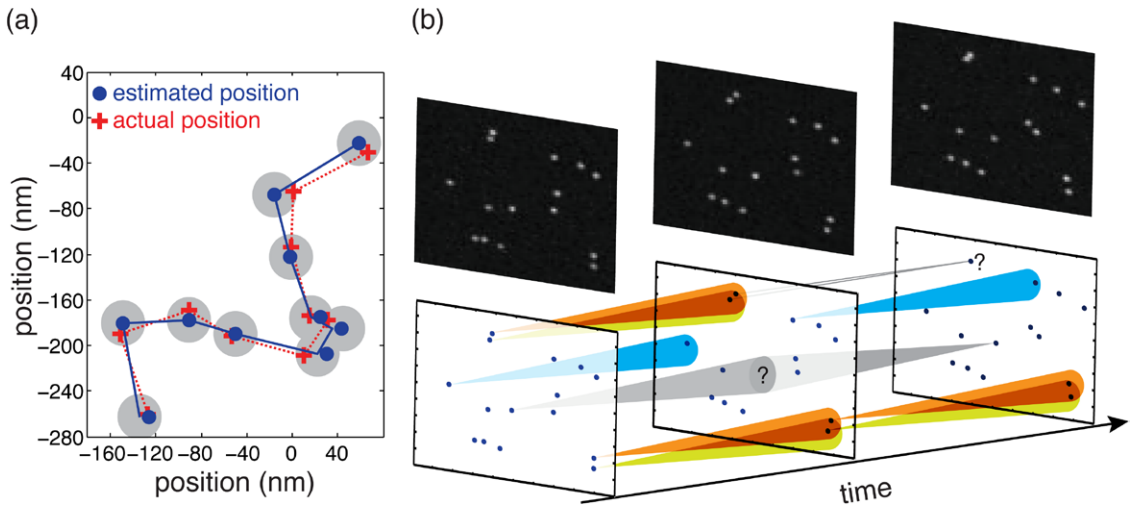

Figure 5. Localizations linking and trajectory reconstruction. (a) Estimations of the position of a diffusing particle (blue dots) obtained from successive frames are reconnected to build up a single-particle trajectory. The actual particle positions are shown as red circles. The gray shaded circles correspond to the localization precision. (b) Representative frames of an SPT movie including several fluorescent particles and schematic representation of the principles of the localization linking algorithm. While relatively sparse localizations are easily reconnected (cyan cones), the algorithms must contemplate the possibility of dealing with ambiguities arising from closely spaced localizations (yellow/orange cones), blinking emitters (gray cones) and missed localizations (gray lines).

148, 150, 163–174]. The optimization might be performed by means of several approaches, some of which were originally developed for air surveillance radar systems, including the use of Viterbi or greedy algorithms, and Karman filtering. A powerful method consists of multiple hypothesis tracking (MHT). MHT is a deferred decision logic in which alternative data association hypotheses are formed whenever observation-to-track conflict situations occur and multiple competing hypotheses are represented in a tree structure. MHT is designed for situations in which the target motion model is very unpredictable, as all potential track updates are considered. To limit the complexity of the reconnection combinatorics for reasons of finite computer memory and computational power, MHT typically includes approaches for deleting the most unlikely potential track updates [150, 165–168].

Particle linking can be also performed simultaneously with the localization step, or the two procedures can be iteratively applied to progressively refine their respective outputs (see for example the description of Method 10 in [21]). In addition to particle positions, information about the fluorescence intensity, PSF shape as well as models of the type of particle motion and emitter photophysics can also be included in the linking routine to improve reconnection performances [150, 171]. From a recent evaluation of several tracking algorithms, it emerged that the use of prior knowledge about the particle's type of motion is a key factor for tracking reliability [21]. Therefore, when analyzing SPT data, it is advisable to generate synthetic training-data to tune the algorithm parameters for each experimental condition.

3.3. Trajectory analysis and interpretation

Once the data processing of SPT is performed and the reconnected trajectories are obtained, the final step involves analyzing the trajectory, testing particle dynamics and describing them in terms of the type of motion and quantifying the diffusion parameters.

The most common approach for the analysis of single molecule trajectories consists of the calculation of the mean square displacement (MSD), describing the average extent of space explored by a particle as a function of the time lag t_{lag}. For a particle j diffusing in 3D, whose position coordinates $\boldsymbol{x}_j = \{x_j, y_j, z_j\}$ are sampled at N discrete times $m\Delta t$, the MSD for a single trajectory is calculated as:

$$\mathrm{MSD}(t_{\mathrm{lag}} = m\Delta t) = \frac{1}{N-m}\sum_{i=1}^{N-m}[\boldsymbol{x}_j(t_i + m\Delta t) - \boldsymbol{x}_j(t_i)]^2. \tag{3}$$

An example of how the MSD calculation is performed is provided in figures 6(a) and (b) for the 2D case. It should be noticed that the MSD in equation (3) is calculated assuming the equivalence of displacements calculated at different times t_i and therefore it represents a time-average. For this reason, in section 5, we will refer to this quantity as T-MSD in order to distinguish it from the ensemble-averaged (E-MSD) and time-ensemble-averaged MSDs (TE-MSD). The MSD is typically plotted versus t_{lag} on either a linear–linear or log–log scale (figures 6(b)–(d)). The dependence of the MSD with t_{lag} is related to the type of motion performed by the particle. Different authors [60, 69–75] derived theoretical expressions for the dependence of the MSD on t_{lag} for particles moving under different conditions (figures 6(c) and (d)). For Brownian diffusion, the MSD can be calculated as the variance of the solution of the diffusion equation [47] and it can be shown to scale linearly with t_{lag}:

$$\mathrm{MSD}(t_{\mathrm{lag}}) = 2dDt_{\mathrm{lag}}, \tag{4}$$

where d represents the dimensionality of the space in which the motion takes place and D is the diffusion coefficient.

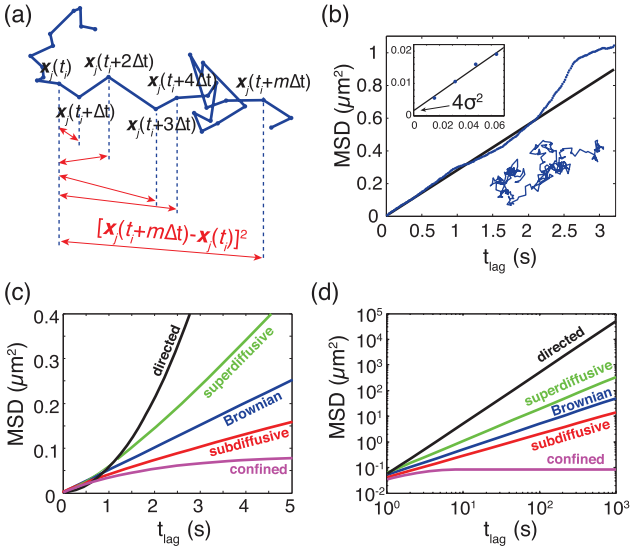

Figure 6. Trajectory analysis and MSD curves. (a) Schematic representation of the calculation of the square displacement of a 2D trajectory for a given initial time t_i and different t_{lag}. (b) Time-averaged MSD of a single particle trajectory in 2D, as a function of the time lag. Due to the finite trajectory length, the MSD curve at large t_{lag} has poor statistics and deviates from linearity. Estimation of the diffusion coefficient can be obtained by fitting of the short t_{lag} region of the MSD plot [180]. The fit must take into account the effect of the localization indetermination, which produces a nonzero offset in the MSD curve (inset). (c), (d) Plot the MSD on linear (c) and log–log scale (d) for representative types of diffusion in 2D. Brownian diffusion shows a linear behavior. Anomalous diffusion displays power-law behavior and, depending on the value of the scaling exponent, can be classified into sub- or super-diffusion. Directed motion, corresponding to the superimposition of Brownian and ballistic motion, is characterized by a quadratic scaling. Confined motion shows, after an equilibration time, saturation to a characteristic plateau, whose value is proportional to the confinement area.

However, different scaling of the MSD can occur in practice as a consequence of the heterogeneous environment in which particles diffuse and of interactions with surrounding components [20, 75, 96, 175]. In many biological systems, it has been observed that particles often display anomalous diffusion, described by a power-law scaling:

$$\mathrm{MSD}(t_{\mathrm{lag}}) = 2dKt_{\mathrm{lag}}^{\alpha}. \tag{5}$$

In equation (5), K is a generalized diffusion constant with fractional dimensions of $[l]^2[t]^{-\alpha}$ and α is the so-called anomalous exponent. In comparison with the Brownian diffusion, the case in which $\alpha < 1$ is usually referred to as sub-diffusion, whereas $\alpha > 1$ is called super-diffusion. Another important type of motion observed in biological systems is the directed motion:

$$\mathrm{MSD}(t_{\mathrm{lag}}) = 2dDt_{\mathrm{lag}} + (vt_{\mathrm{lag}})^2, \tag{6}$$

characterized by a ballistic movement or active transport with speed v, and observed for the motion of molecular motors and active transport along microtubules [20, 164, 176].

A confined type of diffusion, due to the presence of compartments constraining particle diffusion within finite regions of space has also been observed and described [177–179]. Although in this case the exact dependence of the MSD on t_{lag} depends on the shape of the confining region and on the dimensionality of the space, the general effect of this confinement is to produce a plateau in the MSD curve at large t_{lag} and a useful formula approximating this behavior in 2D is given by [178]:

$$\mathrm{MSD}(t_{\mathrm{lag}}) = \frac{L^2}{3}\left(1 - \exp\left(-\frac{t_{\mathrm{lag}}}{\tau}\right)\right), \tag{7}$$

where L is the linear dimension of the confinement region and τ represents a characteristic equilibration time after which the effect of boundaries appears and the MSD saturates.

For particles experiencing only one type of motion during the observation time, a possible way of classification is by comparing the scaling of the experimental MSD with predictions from different motion models. Fitting of the MSD can be performed by means of a suitable model, thus allowing the quantitative estimation of diffusion parameters. However, care should be taken when fitting the MSD for the determination of the type of motion as well as obtaining parameters such as the diffusion coefficient or the anomalous exponent [20, 180–185].

An important factor to take into account when analyzing the MSD curves is the effect of the inherent localization precision in the particle position. In fact, the finite localization precision adds a constant term to the MSD, which, if not properly accounted for, can limit or bias the exact quantification and interpretation of the MSD data [20, 180–184]. In addition, although each data point in the MSD plot is the result of an average over different times t_i, because of the finite trajectory length, at large time lags this average is performed over a smaller number of data (equation (3)), resulting in more scattered data points and less statistical significance [186], as shown in figure 6(b). In this case, it becomes challenging to unambiguously classify the type of motion. For the calculation of diffusion parameters, fitting must be performed over a limited number of points having larger statistics [180, 181, 184]. To increase the statistics, the (time-averaged) MSD can be further averaged over the ensemble composed by J multiple trajectories, thus providing the time-ensemble-averaged MSD:

$$\mathrm{TE\text{-}MSD}(t_{\mathrm{lag}} = m\Delta t) = \frac{1}{J}\frac{1}{N-m}\sum_{j=1}^{J}\sum_{i=1}^{N-m} [\boldsymbol{x}_j(t_i + m\Delta t) - \boldsymbol{x}_j(t_i)]^2. \tag{8}$$

Although the additional averaging has the effect of smoothening the MSD curve at large t_{lag}, it prevents the detection of heterogeneities in the populations of particles, thus only allowing calculation of ensemble-averaged behavior and diffusion parameters. However, differences in diffusive behavior between subsets of ensembles of particles can still be globally extracted by considering the full distribution of displacements and its fitting to a mixed model [187]. A similar approach has also been applied to the detection and classification of mixed diffusion types within a long single-particle trajectory [188]. Recently, methods have also been

developed to allow unbiased trajectory classification based on the moment scaling spectrum [189, 190] or Bayesian inference [191], as well as to optimally calculate the particle diffusion constant and trapping energy [192, 193]. In parallel, alternative estimators have also been proposed for trajectory classification, such as the distribution of directional changes [194], as well as for the calculation of the anomalous exponent, via the mean maximum excursion approach [195] or the fractionally integrated moving average (FIMA) framework [185].

A main interest in biophysics consists of the study of the occurrence of spatiotemporal heterogeneity in the motion of diffusing particles, due to interactions with the surrounding environment. Therefore, in recent years, considerable effort has been devoted to the detection of transient changes of motion or diffusivity within the same trajectory, and to the visualization of spatial regions with different dynamic properties. Time-dependent changes might be detected by means of methods involving trajectory segmentation, obtained via classification parameters calculated over the trajectory with temporal sliding windows [196, 197], by supervised classification [198], Bayesian algorithms [199, 200] or the Hidden Markov Method [201]. In addition, high-density tracking techniques such as multicolor SPT, sptPALM or uPAINT, coupled with suitable analysis methods [68, 74, 88, 93, 202–204] have begun to provide spatially resolved information about particle dynamics and have potential for understanding several space-dependent diffusive mechanisms that drive complex phenomena in living systems.

4. Selected biological applications of SPT

4.1. Studies of cell membrane dynamics and organization

The cell membrane of living cells separates the interior of the cell from its external environment and controls the passage of substances into and out of the cell. It consists of a phospholipid layer and embedded proteins. Importantly, cells communicate with each other and with their external environment through specific proteins (called receptors) expressed on the cell membrane, enabling the cells to perform highly specialized biological functions. Once considered a relatively unstructured 'sea' of lipids and proteins potentially able to form aggregates [205], the cell membrane is now widely accepted as being highly dynamic and compartmentalized, thus allowing lipids and proteins to be organized in specific regions of varying size and composition [206–208]. Since its invention, SPT has crucially contributed to the discovery of this dynamic organization at multiple spatiotemporal scales and, notably, has evidenced its importance for regulating a large variety of cellular processes. Given the vast amount of published SPT studies on the cell membrane of multiple different cell types, it would be virtually impossible to thoroughly review all these studies here. Thus, we highlight some of the most salient examples in which SPT has contributed to the investigation of cell membrane dynamics and organization. For further information, the reader is referred to several excellent reviews of the topic [30, 32, 38, 206, 209–211].

The investigation of the cell membrane by SPT has mainly focused on two major subjects, sometimes highly interconnected. One general topic concerns the actual dynamic organization of the cell membrane from fundamental questions that address how and why this organization is so persistent at different spatial and temporal scales, to a myriad of different studies aiming at deciphering the 'molecular organizers' that are responsible for this non-random distribution. The second topic is highly biologically oriented, as these studies are related to particular protein receptors performing specific cellular functions, with a focus on investigating their spatiotemporal dynamic organization, how this organization translates into receptor and cell function and elucidating the molecular mechanisms responsible for this organization.

From numerous studies performed for more than 20 years, it has become clear that lipids and proteins in the cell membrane exhibit very complex dynamics, often accompanied by anomalous diffusion. Moreover, the diffusive properties often change over a wide range of sizes, from tens to hundreds of nanometers, and durations, from a few milliseconds to seconds [38, 206]. This complex behavior is caused by a combination of reasons including molecular crowding, specific molecular interactions, membrane topology and interactions with nanostructures within the membrane, i.e. caveloa, clathrin coated pits and lipid rafts (figure 7). Moreover, the cell membrane contains physical links to both the extracellular space (via the glycocalyx matrix) and the cytoplasm (the immediate actin cytoskeleton) that can act as barriers to the translational diffusion of molecules within the lipid bilayer of the membrane.

In broad terms, the most recent view on the cell membrane considers that its dynamic organization is highly hierarchical with different molecular organizers working in synergy at different spatial scales (reviewed in [32, 206, 210, 212, 213]). A first level of membrane compartmentalization might be provided by cholesterol-enriched nanodomains, also termed 'lipid rafts'. Aside from cholesterol, these small nanodomains (~3–15 nm in size) contain specific types of lipids and proteins involved in signaling (glycosylphosphatylinositol-anchored proteins, GPI-AP, reviewed in [212]). Different biophysical techniques, including SPT, have indicated that many raft nanodomains are extremely dynamic and short-lived, and their constituent molecules can be recruited very transiently, in the order of a few to approximately several hundred milliseconds [210, 211, 214]. Their small and transient lifetime is the main reason why a considerable number of researchers in the field do not yet believe in the existence of these nanodomains, or that cholesterol is responsible for the nanodomain formation of lipids or proteins such as GPI-APs. In fact, recent studies from Mayor's group suggest that short-lived 'actin asters' (short actin filaments driven into asters by myosin motors) in the close proximity of the inner cell membrane are instead responsible for transient GPI-AP aggregation at the nanoscale [215]. Unfortunately, the actin-aster hypothesis has also been difficult to prove given the supposedly small size and dynamic nature of these asters [215, 216].

A second level of compartmentalization appears to be formed by the actin membrane skeleton in close proximity to the inner cell membrane (reviewed in [38]). This model

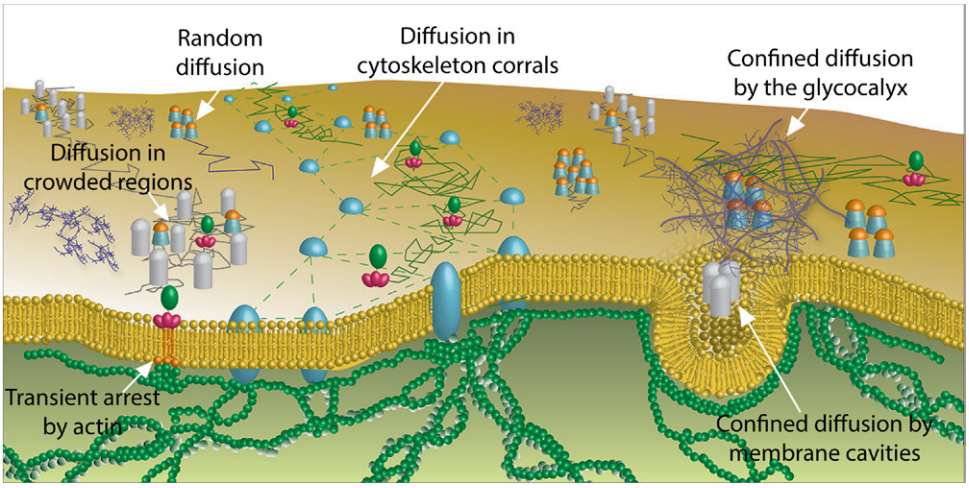

Figure 7. Schematic representation of the diverse lateral diffusion of molecular components on the cell surface. Different molecular actors contribute to the confined or anomalous diffusion of molecules: molecular crowding, skeleton corrals, membrane cavities such as clathrin-coated pits or the glycocyalyx matrix. These molecular components can also induce the transient arrest of receptors, including the immediate cortical actin cytoskeleton.

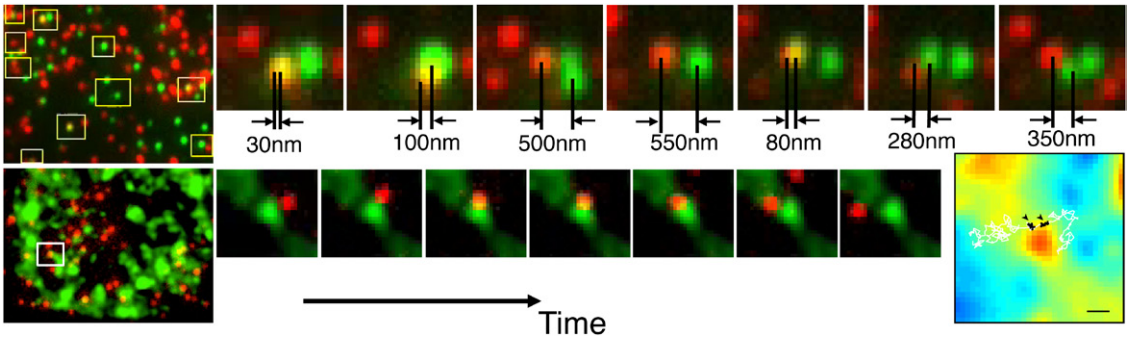

Figure 8. Dual-color SPT examples to determine dynamic interactions between molecular components of the cell membrane. In the upper raw two different QDs (red and green) are used to map dynamic interactions between similar receptors. In this example, the QDs diffuse around in space but remain confined in regions smaller than 1 μm in size. By measuring the mutual distance between adjacent QDs as a function of time one can determine the actual size of the corral region. The left (larger) panel shows a still frame of multiple red- and green-labeled receptors. The yellow squares identify regions where two QDs come closer to each other. The sequential (smaller) frames show different positions of two QDs. The lower panel shows QD-labeled receptors (red spots) exploring regions enriched by clathrin (green). The sequential zoom-in frames illustrate periods of random diffusion interleaved with transient arrest of receptor mobility upon interaction with clathrin. The right-most panel shows an enlarged color-coded image of the sequential frames. The clathrin intensity is color-coded (from blue to red as the clathrin intensity signal increases). The diffusing trajectory (white) is super-imposed on top of the clathrin image. The black dots (and arrows) on the trajectory point to regions of transient arrest of receptor mobility [203].

originated over three decades ago based on lateral diffusion studies of proteins in the membranes of red blood cells [217] and was later expanded by work in the Kusumi Lab [38]. By means of 40 nm-gold particles and temporal sampling rates of 40–50 kHz, the Kusumi lab showed that virtually all the molecular components of the cell membrane, i.e. lipids, GPI-APs and transmembrane proteins, are confined in compartments of ~30–250 nm in size, for average residence times between ~1–20 ms [22, 38]. This confinement appears to be imposed by the actin cytoskeleton. Thus, according to this model the long-range diffusion of molecules is restricted because it is rate-limited by fluctuations in the cytoskeletal structure. These fluctuations in turn allow the inter-compartmental barriers to be traversed by the moving molecule, in a 'hop-diffusion' manner [22]. By contrast, short-range diffusion within each compartment is much more rapid and can be ascribed to Brownian motion.

The association between similar protein species resulting in protein complexes or nanoclusters provides a third level of organization. These complexes may interact with lipid rafts [212, 218–220], the actin cytoskeleton [221–226], and/or with other membrane structures on the cell surface [90, 203, 227, 228]. Information on these processes has been mostly gathered by correlating the diffusion dynamics of labeled molecules with respect to the actual position of membrane structures labeled with organic dyes or autofluorescent proteins (figure 8). For instance, using a combination of QD-receptor tracking and GFP-tagged actin, Lidke and co-workers showed that actin filament bundles define micrometer-sized domains that confine mobile receptors on the cell membrane. Dynamic reorganization of actin structures occurs over seconds, making the location and dimensions of actin-defined domains time-dependent [221]. The involvement of the actin cytoskeleton actively regulating the diffusion of membrane receptors appears in

fact to be a rather general theme, as different receptors have shown reduced mobility, transient trapping and/or anomalous diffusion by their interaction with cytoskeletal structures [89, 221–226, 229]. A similar dual-color approach has been used to reveal interactions between the labeled receptor with other membrane structures such as lipid nanodomains [188], clathrin coated pits [228] or the glycocalyx matrix [203].

Dual-color SPT has also been extended to the examination of correlated diffusion between similar or distinct molecules to study the dynamics of protein–protein interactions at the single molecule level. The co-diffusion of single molecules allows the distinction of colocalization and molecular interactions since co-movement is a strong signature of a physical link (direct or indirect) between two molecules. Moreover, the lifetime of the interaction or formed complex can be directly obtained by measuring the lengths that the dual trajectories exhibit correlated motion. This approach has been exploited to visualize dynamic interactions between the same specie of receptors [201, 229, 230] or to reveal the meso-scale compartmentalization of receptors, as the mutual distances between two labeled receptors remain co-confined in space (figure 8) [203].

In the field of neurobiology, SPT has become one of the complementary methods for the study of the molecular mechanisms involved in the regulation of neuronal activity (see reviews in [30, 31]). From a large number of SPT studies on different neuroreceptors it has become now widely accepted that neuronal surface mobility and its regulation constitutes one of the crucial factors contributing to synaptic plasticity. For more insight into the different neuroreceptors investigated so far, the reader is referred to recent excellent reviews on the topic [30, 31, 231, 232]. In summary, a wealth of SPT experiments together with other biophysical and bio-functional essays have completely changed our notion of the cell membrane and have highlighted the crucial role of cell membrane organization and dynamics regulating cellular function. As techniques further mature, many of the remaining controversies regarding the nature of nano-compartmentalization on living cell membranes are expected to be resolved.

4.2. Intracellular studies with SPT

Different intracellular processes, including virus internalization, signaling, molecular transport, chromatin dynamics and gene regulation have already been addressed using SPT. In the case of viruses, SPT has been extremely powerful in obtaining the mechanistic details of their internalization process. For instance, the Zhuang Lab followed the fate of the influenza virus (the virus that causes flu) by loading the viral membrane of the virus with a self-quenching dye (using high labeling concentrations) [233]. By tracking the motion of the individually labeled viruses and measuring their instantaneous velocities as a function of time, the authors identified different phases of motion from the first contact of the virus with the cell membrane, translocation into the perinuclear region in a directed-type of motion and finally fusion in the nuclear periphery. Moreover, by applying dual-color labeling the authors identified the routes by which influenza viruses are internalized by cells, providing mechanistic details of the process [234]. Similar SPT studies have been performed to elucidate the entry and internalization pathways followed by other viruses, including the HIV virus on cells of the immune system (see [87, 190, 235, 236] and reviews [43, 59]).

Understanding the mechanisms by which membrane proteins are internalized and transported upon activation is crucial to understanding signaling pathways. For these purposes QDs can be functionalized with receptor ligands and exploited to activate cell membrane receptors. By following their fate as they become internalized, details on their complex trafficking and internalization mechanisms into different intracellular compartments has been obtained [237–240]. Moreover, the first studies by SPT on the dynamic properties of different intracellular molecules, for instance, molecular motors involved in cellular transport and division, have been already reported [35, 241, 242]. Recently, the combination of super-resolution microscopy and SPT has allowed the first studies of cargo transport along microtubules inside cells [176] and the dynamic organization of protein complexes in sub-cellular organelles such as mitochondria [93].

SPT is also starting to provide understanding of the internal structure and dynamics of molecules inside the cell nucleus. The labeling of specific nuclear structures using antibodies or autofluorescent proteins has revealed in recent years a complex spatiotemporal nuclear organization, with distinct sub-compartments highly specialized in terms of function (for reviews see [243, 244]). Moreover, dynamic studies using some of the techniques described in section 2 have shown that the nuclear interior is highly crowded and structured, so that the diffusion of molecules inside the nucleus can be highly complex, with periods of slow Brownian diffusion, interleaved with directed motion and/or restricted diffusion (see review [37]). For instance, using two-photon microscopy together with orbital tracking (described in section 2.3.2) the Gratton Lab showed that chromatin inside the nucleus undergoes regions of confined Brownian motion, alternated by periods of fast curvilinear motion and diffusional jumps [97]. These short periods of diffusional jumps have been associated with the active transport of chromatin inside the nucleus [245]. Recently, a combination of reflected light sheet microscopy and SPT using autofluorescent proteins has been implemented to measure the dynamic properties of individual transcription factors in the nucleus of living cells [34]. Moreover, using dual-color SPT the researchers could directly observe spatiotemporal colocalization between different transcription factors and their co-activators [34]. In another recent work, Izeddin and co-workers combined HILO illumination with sptPALM to investigate the dynamics of different transcription factors as a function of the nuclear geometry, establishing a link between the kinetics of transcription-factor-target-search and the nuclear architecture for gene regulation [246]. Although SPT studies inside cells are considerably less abundant that research on cell membranes given the increased complexity of the experimental conditions, as the technique matures and more efficient labeling methods are developed to target intracellular molecules, we expect that the range of intracellular studies will increase dramatically in the years to come.

5. Theory and modeling

Although the observation of diffusion processes can be dated back to the description of the motion of dust particles in air provided by Titus Lucretius in his didactic poem Nature of Things written c. 60 BC [247], the first systematic SPT experiments were performed at the beginning of the twentieth century by Perrin [248] and Nordlund [249]. However, a few years before these experiments, Einstein [250] and Langevin [251] had already derived two theoretical formulations of Brownian motion, showing that the motion of pollen grains in water observed by Robert Brown in 1828 [252] was caused by the thermal movement of the surrounding liquid molecules. In Einstein's theory, the solution of diffusion equation is a normalized Gaussian distribution, whose variance scales linearly in time and provides the MSD (equation (4)). In his formulation, Einstein's theory considers three fundamental assumptions: (i) the particles are independent; (ii) particle displacements are statistically independent and uncorrelated; and (iii) particle displacements correspond to random kicks by water molecules with no preferential direction and the distributions of step lengths and waiting times have a finite mean and variance [47, 253, 254]. Einstein's model was successively associated with the theory of random walk [255] by Smoluchowsky [256]. The equivalence of the diffusion of an ensemble of particles with the random walk of an individual one shows that the process is ergodic, i.e. following a single representative particle over a long time provides the same information about an ensemble as monitoring the ensemble itself. The assumption of ergodicity is considered in many experimental approaches, including SPT, to be an essential characteristic of diffusion. However, several SPT experiments have shown deviation from Brownian diffusion, with a power-law scaling of the T-MSD (anomalous diffusion). Besides anomalous diffusion, SPT measurements in living cells have recently displayed irreproducibility in the T-MSD curves calculated for different trajectories of identical molecules, challenging the ergodic hypothesis and opening up new questions about their implications for cell biology. In the following, we will review the most accepted theoretical models of anomalous diffusion, their connection with ergodicity breaking and examples of the observation of anomalous and nonergodic dynamics in living systems.

5.1. Models of anomalous diffusion

One of the most important results obtained by means of SPT is the observation and measurement of deviation from pure Brownian behavior [257]. Similar deviations have been also reported for diffusion in several complex media [187], including biological systems [46, 258]. Measurements of single particle trajectories in living cells have in fact shown that the MSD displays nonlinear scaling, associated with a variety of types of motion. Besides (normal) Brownian diffusion, particles can exhibit directed motion, confined motion, anomalous diffusion and transient immobilization [20, 75]. In general, these different types of motion result from the interaction of the particle with the environment. Their study can reveal a variety of information regarding the properties of the environment, as well as on the kinetics of reaction with molecular binding partners, the presence of structures affecting particle diffusion or the role of molecular motors. In order to interpret these different behaviors and to take advantage of single particle trajectories to obtain information on the surrounding media, considerable theoretical effort has been made to describe diffusion in complex systems.

Anomalous diffusion can originate from several mechanisms, and its causes have been widely studied theoretically by means of both numerical [259, 260] and analytical methods [47, 261–265]. Anomalous diffusion typically refers to the power law-form of the MSD as given in equation (5). The value of the anomalous exponent a is used to further distinguish between subdiffusion ($0 < \alpha < 1$) and superdiffusion ($\alpha > 1$). Generally speaking, anomalous diffusion is a consequence of the violation of at least one of the assumptions of Einstein's theory, thus producing deviation from the central limit theorem [20, 47]. For example, anomalous diffusion might result from pathologically broad distributions of jump times or jump lengths, or strong correlations in diffusive motion [20].

Several models of anomalous diffusion have been proposed for the evaluation and interpretation of SPT data. However, assessing what mechanisms cause anomalous diffusion in the experimental data is not straightforward and requires the evaluation of several parameters [266]. Many of the models producing anomalous diffusion have been recently reviewed and thorough mathematical detail can be found in [47, 49, 175]. In the following, we will provide a brief description of some classes of models describing anomalous diffusion and their application to biophysical systems.

A first example of anomalous diffusion is provided by the continuous time random walk (CTRW) [267] (figures 9(a)–(c)). The CTRW consists of a generalization of the classical random walk [255] in which both the waiting time and the step length might be continuous random variables. The CTRW can produce subdiffusive or superdiffusive behavior depending on whether the average waiting time and the variance of the distribution of step lengths are finite or infinite. While a waiting time distribution with diverging mean produces subdiffusion (figures 9(a)–(c)), the CTRW is superdiffusive if the step length distribution has infinite variance (Levy flight). Other forms of CTRW arise when the waiting time and step length are coupled, such as the Levy walk [47]. In a biophysical context, the subdiffusive CTRW can be interpreted as a diffusive motion in the presence of traps [260], e.g. due to biochemical binding of the diffuser with immobile structures.

A second model leading to anomalous diffusion is fractional Brownian motion (FBM) [268], a self-similar Gaussian process with stationary increments. In FBM, successive increments are correlated, thus violating the Markovian assumption and introducing memory effects. FBM was introduced by Mandelbrot in the 1960s [268]. The anomalous exponent of FBM is linked to the so-called Hurst coefficient via the relationship $\alpha = 2H$, with $0 < H < 1$. FBM is particularly relevant for the case of subdiffusion ($\alpha < 1$, $H < 0.5$), where the anticorrelated motion can be associated with the viscoelastic properties of the environment in which the particles diffuse

[269]. Within the context of living cells, viscoelasticity can be induced by macromolecular crowding and/or transient interactions among cellular components [175].

Another model of anomalous diffusion involves transport on fractal structures [270]. Fractals are self-similar objects whose size depends on the scale one applies to measure them and, therefore, do not have a characteristic size [270]. Although it is possible to built exact mathematical fractals by iterating the same structure at different scales, many natural objects show self-similarity in a statistical sense, meaning that their overall size depends, at least within a range of scales, as a power law of the scale used to measure them. The exponent of this power law is referred to as fractal dimension d_f and is different from the dimensionality of the space in which the object is embedded. The space exploration of a random walker moving on a fractal structure is highly impacted on the fractal geometry of the accessible space and the corresponding MSD shows anomalous diffusion with exponent $\alpha = 2/d_w$, where d_w is the walk dimension and it can be shown to be larger than d_f. A useful approach for the description of diffusion on a fractal is represented by the percolation model, providing a mathematical description of random fractals [271]. The percolation model is obtained by filling random points on a lattice with a given probability of occupation. These points represent inaccessible areas (or obstacles) for the motion of the random walker. Subdiffusion caused by hindering obstacles is often used to describe molecular crowding in cells, caused by the presence of organelles, macromolecular complexes and biopolymers [272]. At a critical probability, called the percolation threshold, the density of filled points will reach a value such that they will form an 'infinite' cluster, i.e. a connected region spanning the whole space. In this condition, the accessible space will show fractal geometry, and the walker performs anomalous diffusion [273]. Even in a region slightly below the critical threshold, this model predicts deviation from Brownian diffusion due to immobile obstacles. In this regime, a region of anomalous diffusion is still observed at short times. Above a crossover time, the linear behavior is restored. The crossover time increases with the probability of occupation until, at the percolation threshold, anomalous diffusion occurs at all time scales [259].

Finally, anomalous diffusion can be obtained by assuming a time-dependent or space-dependent diffusivity, such as in the scaled Brownian diffusion [274] or in heterogeneous diffusion processes [275–277]. These processes include cases in which the diffusivity is expressed as a continuous function (generally a power law) of either the time (scaled Brownian motion) or the spatial coordinates. As an example of the latter kind of process, a position-dependent diffusivity was observed in living cytoplasm as a function of the distance to the nucleus [278]. Recently, a new family of heterogeneous diffusion processes (called *patch* models) has been proposed, involving a walk in a landscape with randomly switching diffusivity, either in a time- or space-dependent manner [279]. This model was found particularly relevant to describe the diffusion in heterogeneous landscapes, such as the plasma membrane of living cells [53].

5.2. (Weak) ergodicity breaking and anomalous diffusion

According to the ergodic hypothesis, observables calculated from measuring a single particle for a long time are equivalent to the same observables calculated over a large number of particles at a given time. Thus, the time and ensemble averages are the same. However, when tracking chemically identical molecules diffusing in cells, one often finds that time averages (e.g. the T-MSD) calculated over different particles vary in amplitude, independently of the observation time [50–53, 280, 281]. In these cases, time averages remain random variables and hence are irreproducible [50–53, 280], leading to the breakdown of the central limit theorem and nonergodic behavior. The scattering between the T-MSDs of individual trajectories (see for example figure 9(d)), can be used to calculate the so-called ergodicity breaking (EB) parameter [266, 282, 283], i.e. the ratio between the variance and the squared mean of the T-MSD at any given time t_{lag}, in order to quantify the level of nonergodicity of the system.

The different amplitudes of the T-MSD for trajectories of chemically identical molecules can be caused by a limited exploration of regions of the phase space characterized by different dynamic properties, as a consequence of structural modifications (e.g. change in conformational state, co- or post-translational modification, ligand binding) or interactions with the surrounding environment (e.g. confinement within actin cytoskeleton domains), lasting longer than the measurement time. Therefore, even in the limit of an infinitely long trajectory, the time-averaged MSD (T-MSD, equation (3)) is not equivalent to the ensemble-averaged MSD (E-MSD, figures 9(d) and (e)), which, using the same notation as in section 3, can be calculated for any initial time t_i as:

$$\text{E-MSD}(t_{lag} = m\Delta t) = \frac{1}{J}\sum_{j=1}^{J} [\boldsymbol{x}_j(t_i + m\Delta t) - \boldsymbol{x}_j(t_i)]^2. \quad (9)$$

For some of the models described in the previous section (such as the CTRW and the heterogeneous diffusion models), anomalous diffusion is connected with weakly nonergodic behavior [47–49]. The term weak-ergodicity breaking was first introduced by Bouchaud for physical glasses [265], to differentiate this behavior from the 'strong' nonergodic case, in which the phase space is divided in nonconnected domains and each trajectory explores only one of them. In contrast, weak ergodicity breaking is characterized by a fully connected phase space and the systems can access the whole phase space independently of the starting point. However, the occupation fraction of a state is not equal to the fraction of the system in the ensemble occupying the same state [284]. This leads to an infinite exploration time of the whole phase space and thus, although accessible domains of the phase space are connected, a single trajectory will never explore them all, no matter how long one measures. Weak ergodicity breaking has been observed experimentally for various systems [50–53]. From the theoretical point of view, this behavior is characteristic of the subdiffusive CTRW and of the models of time-dependent or space-dependent diffusivity [47].

In these cases, the time-averaged MSD shows linear scaling in t_{lag}, as does the time-ensemble averaged MSD (figure 9(d)). This might erroneously lead to the conclusion that the motion is normal Brownian diffusion. However, the evaluation of the ensemble-averaged MSD shows anomalous behavior t_{lag}^{α} and thus nonergodicity (figure 9(e)). Another important characteristic associated with the weak ergodicity breaking is aging, i.e. a power law dependence of the time-ensemble-averaged MSD on the measurement time. Recasting $N = T/\Delta t$ in equation (8), the time-ensemble-averaged MSD shows an explicit dependence on the observation time T. For the models showing weak-ergodicity breaking, it can be demonstrated [47] that the time-ensemble-averaged MSD scales as $T^{\alpha-1}$, where α is the anomalous exponent, and therefore never reaches a plateau (figure 9(f)).

5.3. Evidence of anomalous diffusion and weak ergodicity breaking in living systems

Anomalous diffusion has been widely observed in living systems and is generally associated with the effect of molecular crowding [46], producing obstacles to diffusion and traps with a distribution of binding energies or escape times [20], or heterogeneity in the interaction with the environment. A huge number of examples of anomalous diffusion for different molecular or supramolecular components in different cell types and cellular compartments has been reported in the literature. The extensive description of these examples goes beyond the scope of this contribution and has been thoroughly reviewed elsewhere (see e.g. [20]). In the following, we will focus our attention on a few recent examples in which SPT experiments have revealed the occurrence of anomalous diffusion in connection with weak ergodicity breaking.

The first evidences of weak ergodicity breaking in the dynamics of living cell components were provided almost simultaneously in two seminal works, both published in 2011 [50, 52]. In the first of these works, Jeon and co-workers studied the diffusion of lipid granules in yeast cells by combining SPT and optical tweezer experiments [52]. The T-MSD from individual trajectories of lipid granules displayed a complex dynamics composed by a nearly linear behavior at short time lags, followed by subdiffusive motion at longer times. The short-time data displayed weak ergodicity breaking (i.e. the non-equivalence of T-MSD and E-MSD) and large scattering of the T-MSD amplitudes. This behavior was found to be compatible with the CTRW model, whereas at long times the resulting motion was interpreted within the framework of the FBM. However, in contrast to CTRW, no aging was observed. The authors argued that the lack of aging could have been caused by the presence of a natural cutoff in the power-law waiting time distribution and proposed the binding to semi-flexible cytoskeletal filaments as a physical mechanism to interpret their results.

In the second work, Weigel *et al* [50] performed tracking of the Kv2.1 potassium channel in the plasma membrane of HEK cells. In this case, the T-MSDs also showed a wide scattering of amplitude and a different scaling as compared to E-MSD. In addition, the T-MSDs presented a power law

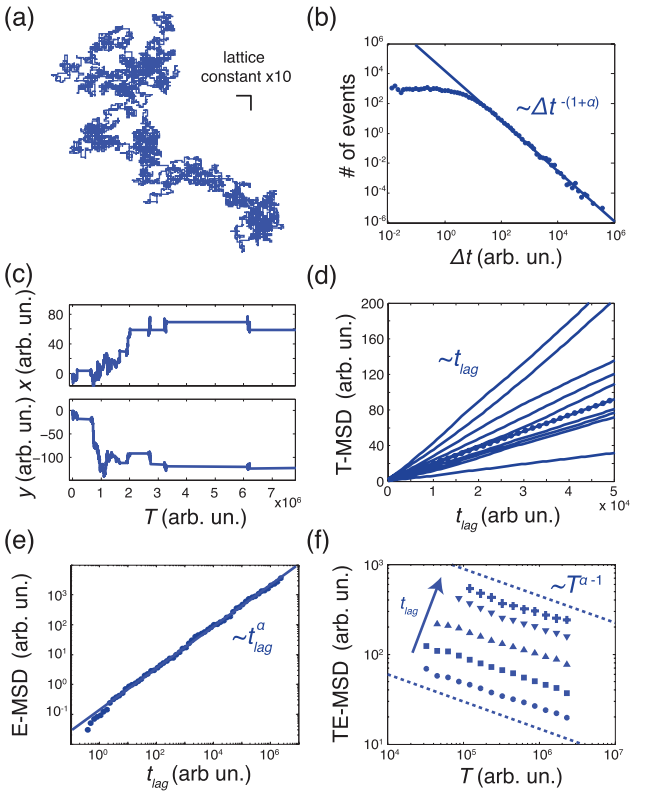

Figure 9. Theoretical models of anomalous diffusion and weak-ergodicity breaking: the CTRW model. (a), (c) Lattice-based simulation of a CTRW in 2D. The walker moves on a square lattice. At each move, the walker makes steps of fixed length, given by the lattice constant, in an arbitrary direction (a). The distribution of the waiting time between consecutive steps decays at large time as power-law (b). Plot of the x- and y-coordinates of the walker shows the occurrence of long waiting times (c). (d), (f) The CTRW shows weak-ergodicity breaking, i.e. non-equivalence of time and ensemble averages, and aging, i.e. dependence of the time-ensemble-averaged MSD on the observation time. The time-averaged MSDs of representative CTRW trajectories (blue lines) display linear behavior but a large scattering of amplitudes (d). Although the time-ensemble averaged MSD, denoted by the blue symbols in (d), also scales linearly with the t_{lag}, the ensemble average calculated at $t_i = 0$ has a nonlinear behavior (e). In addition, the time-ensemble averaged MSD calculated at representative t_{lag} has a power law dependence on the observation time, and therefore ages without reaching a plateau (f).

scaling significantly different from 1 at all time scales and the TE-MSD revealed the striking evidence of aging. From the recorded trajectories, the authors identified the occurrence of molecular trapping caused by the transient binding of the Kv2.1 channels to the cytoskeleton and could further measure the power law dependence of the distribution of trapping times. This evidence led them to conclude that the Kv2.1 motion was produced by a CTRW (due to the actin cytoskeleton) on a fractal geometry and to propose that these complex dynamics might be beneficial for regulating membrane compartmentalization and endocytosis.

Weak ergodicity breaking and aging were later observed in the motion of insulin-containing vesicles in pancreatic β cells [51]. Tabei and co-workers demonstrated that this motion can be interpreted through a subordinated scheme, in which CTRW-like behavior due to vesicles binding to microtubules

coexist with FBM caused by fluctuations in molecular crowding or filament network deformation and described its implication for vesicle trafficking, insulin secretion and the resulting pancreatic β cells' function.

Recently, we have shown that nonergodicity and aging also appear in the diffusion of a pathogen-recognition transmembrane receptor in the cell membranes of mammalian cells [53]. In contrast with previous works, the nonergodic behavior of this receptor originates from frequent changes in diffusivity, likely caused by interactions with other molecular components in the plasma membrane and in the extracellular milieu. As such, we could quantitatively reproduce the main features of its dynamics within the framework of a heterogeneous diffusion process (*patch* model) [279]. In addition, our data revealed the correlation between the occurrence of ergodicity breaking with changes in receptor structure and pathogen recognition function [53].

These recent publications have generated a great deal of excitement among theoreticians and biophysicists not only for purely fundamental reasons but, importantly, for the potential implications of nonergodic transport for mechanisms regulating cellular function. On one hand, the complex and heterogeneous environment found in living cells and the inherent spatiotemporal disorder seems to support and justify the occurrence of such 'strange' kinetics [48]. At the same time, new questions naturally arise: How common are these kinetics? Do they form part of an evolutionary strategy? What could they be beneficial for? To answer these questions poses new and stimulating challenges for SPT experiments.

6. Conclusions

SPT studies have demonstrated the importance of performing dynamic experiments in living cells by providing access to single molecule behavior and thereby to a complete statistical characterization of the system under study. From these investigations, we have been able to uncover transport properties in biological processes at nano- and mesoscopic scales. We can now reveal how different parameters related to mobility govern molecular interactions and how they translate into cellular function. These results have immensely advanced our understanding of the mechanisms orchestrating the spatiotemporal organization of molecules in living systems.

SPT has been established for nearly thirty years by now. However, rather than reaching maturity by going through modest developments, the technique is continuously going through tremendous expansion, benefiting from the development of new optical techniques, better labeling strategies and from impressive advancements in molecular biology. Once implemented with large gold colloidal particles, SPT can now be performed with a broad range of fluorescent and non-fluorescent reporters of nanoscopic dimensions, combined with super-solution nanoscopy to increase the number of particles tracked on a single cell to nearly physiological expression levels, and implemented using different illumination schemes to provide access to the full complexity of living cells and even to multi-cellular systems. More complex and sophisticated algorithms for trajectory reconstruction and data analysis are continuously being developed, providing rich insight into different types of molecular transport.

We have summarized the principles of SPT and have tried to follow a chronological order in terms of technological developments, with a focus on novel optical implementations that are predicted to continue in the next few years. Many of them have been driven by the need for accessing more complex structures in living cells, such as intracellular organelles and nuclear compartments. Others are trying to overcome the limitations of fluorescent reporters by developing new optical strategies to detect nanoscopic particles while minimally interfering with the biomolecular process under study. We have described different probes used as SPT reporters, paying particular attention to the trade-off between their optical properties and their suitability to image biological objects with minimum perturbation of the molecule itself and its surroundings. Although the ideal probe, i.e. infinitely stable, bright and with minimal perturbation, does not exist yet, the pace of the development of better labeling strategies and more sensitive detection schemes is huge. Furthermore, the expectation of mapping the motion of individual molecules in living cells without the need for an external label might become reality in a few years from now.

A wealth of information regarding the diffusion of single molecules can be obtained from SPT experiments. We have provided an updated overview on the different algorithms used to reconstruct trajectories and for data analysis, with the main aim of providing the reader with the necessary basic information that is crucial to generate individual trajectories with minimum bias while accounting for the experimental limitations of the system under study. Analyzing SPT trajectories can be a complicated task given the large amount of information contained in the trajectories, so that in practice, novel ways of analyzing the experimental data emerge depending on the process being studied and the parameters the investigator is interested in obtaining. In general, these parameters include types of motion, velocities, association constants, local concentrations or transient interactions between different molecular components. We have highlighted some salient examples in biology where these parameters have been derived to obtain information on the spatiotemporal organization of the cell membrane, intracellular phenomena and nuclear dynamics. The applications of SPT in biology are enormous, and they have been reviewed in many excellent articles cited in this contribution. We have definitely failed to review all of the biological studies performed by SPT but hope that the reader can find here the main lines of biological research currently being undertaken with SPT in combination with other biophysical and biochemical approaches.

From a physics perspective, one of the most astonishing observations derived from SPT studies in biological systems is the fact that anomalous transport governs the diffusion of molecules in living systems. The contribution from theoreticians has also been increasing at a fast pace, from the first theoretical models developed by Saxton in the 1990s to the application of more elaborated models of anomalous transport in recent years. We have summarized the essence of these theoretical models and have further discussed models

that describe ergodicity breaking, another unexpected phenomenon that has become evident from SPT studies in living systems. Whereas the mechanisms that lead to anomalous transport in biophysical systems and consequences for cellular function are being heavily scrutinized, much less is known about ergodicity breaking in biophysical systems. Whether ergodicity breaking is a natural manifestation of the inherent complexity and spatiotemporal heterogeneity of living systems, and/or whether it plays an important role in regulating cell function are yet open questions being addressed by synergistic collaborations between theoreticians and experimentalists.

There is a bright future for SPT research, embracing efforts from molecular biologists, biochemists, engineers and physicists. Many biological questions have already been addressed by SPT, but many other unforeseen observations have also emerged from the use of the technique. In combination with other biochemical and biophysical approaches, SPT should be a powerful tool to connect diffusion and transport at the molecular scale to the dynamic organization of higher-level multi-cellular organisms.

Acknowledgments

We thank J A Torreno-Pina, G J Lapeyre Jr and M Lewenstein for their valuable discussions. Financial support from the Fundació Cellex, the Human Frontier Science Program (Grant No RGP0027/2012), and the Spanish Ministry of Science and Innovation (Grant No MAT2011-22887) is gratefully acknowledged.

References

[1] Reits E A and Neefjes J J 2001 From fixed to FRAP: measuring protein mobility and activity in living cells *Nat. Cell Biol.* **3** E145–7

[2] Lippincott-Schwartz J, Altan-Bonnet N and Patterson G H 2003 Photobleaching and photoactivation: following protein dynamics in living cells *Nat. Cell Biol.* **5** S7–14

[3] Axelrod D, Ravdin P, Koppel D E, Schlessinger J, Webb W W, Elson E L and Podleski T R 1976 Lateral motion of fluorescently labeled acetylcholine receptors in membranes of developing muscle fibers *Proc. Natl Acad. Sci. USA* **73** 4594–8

[4] Haustein E and Schwille P 2007 Fluorescence correlation spectroscopy: novel variations of an established technique *Annu. Rev. Biophys. Biomol. Struct.* **36** 151–69

[5] Elson E L 2011 Fluorescence correlation spectroscopy: past, present, future *Biophys. J.* **101** 2855–70

[6] Kim S A, Heinze K G and Schwille P 2007 Fluorescence correlation spectroscopy in living cells *Nat. Methods* **4** 963–73

[7] Magde D, Elson E and Webb W W 1972 Thermodynamic fluctuations in a reacting system—measurement by fluorescence correlation spectroscopy *Phys. Rev. Lett.* **29** 705–8

[8] Petersen N O, Höddelius P L, Wiseman P W, Seger O and Magnusson K 1993 Quantitation of membrane receptor distributions by image correlation spectroscopy: concept and application *Biophys. J.* **65** 1135–46

[9] Bates I R, Wiseman P W and Hanrahan J W 2006 Investigating membrane protein dynamics in living cells *Biochem. Cell Biol.* **84** 825–31

[10] Eggeling C, Ringemann C, Medda R, Schwarzmann G, Sandhoff K, Polyakova S, Belov V N, Hein B, von Middendorff C and Schönle A 2009 Direct observation of the nanoscale dynamics of membrane lipids in a living cell *Nature* **457** 1159–62

[11] Manzo C, van Zanten T S and Garcia-Parajo M F 2011 Nanoscale fluorescence correlation spectroscopy on intact living cell membranes with NSOM probes *Biophys. J.* **100** L8–10

[12] Holzmeister P, Acuna G P, Grohmann D and Tinnefeld P 2014 Breaking the concentration limit of optical single-molecule detection *Chem. Soc. Rev.* **43** 1014–28

[13] Mivelle M, Zanten T, Manzo C and Garcia-Parajo M F 2014 Nanophotonic approaches for nanoscale imaging and single-molecule detection at ultrahigh concentrations *Microsc. Res. Tech.* **77** 537–45

[14] Zhu P and Craighead H G 2012 Zero-mode waveguides for single-molecule analysis *Annu. Rev. Biophys.* **41** 269–93

[15] Geerts H, De Brabander M, Nuydens R, Geuens S, Moeremans M, De Mey J and Hollenbeck P 1987 Nanovid tracking: a new automatic method for the study of mobility in living cells based on colloidal gold and video microscopy *Biophys. J.* **52** 775–82

[16] De Brabander M, Nuydens R, Geerts H and Hopkins C 1988 Dynamic behavior of the transferrin receptor followed in living epidermoid carcinoma (A431) cells with nanovid microscopy *Cell Motil. Cytoskeleton* **9** 30–47

[17] Gelles J, Schnapp B J and Sheetz M P 1988 Tracking kinesin-driven movements with nanometre-scale precision *Nature* **331** 450–3

[18] Sheetz M P, Turney S, Qian H and Elson E L 1989 Nanometre-level analysis demonstrates that lipid flow does not drive membrane glycoprotein movements *Nature* **340** 284–8

[19] de Brabander M, Nuydens R, Ishihara A, Holifield B, Jacobson K and Geerts H 1991 Lateral diffusion and retrograde movements of individual cell surface components on single motile cells observed with Nanovid microscopy *J. Cell Biol.* **112** 111–24

[20] Saxton M J and Jacobson K 1997 Single-particle tracking: applications to membrane dynamics *Annu. Rev. Biophys. Biomol. Struct.* **26** 373–99

[21] Chenouard N *et al* 2014 Objective comparison of particle tracking methods *Nat. Methods* **11** 281–90

[22] Fujiwara T, Ritchie K, Murakoshi H, Jacobson K and Kusumi A 2002 Phospholipids undergo hop diffusion in compartmentalized cell membrane *J. Cell Biol.* **157** 1071–82

[23] Mie G 1908 Beiträge zur optik trüber medien, speziell kolloidaler metallösungen *Ann. Phys., Lpz.* **330** 377–445

[24] Betzig E and Chichester R J 1993 Single molecules observed by near-field scanning optical microscopy *Science* **262** 1422–5

[25] Sako Y, Minoghchi S and Yanagida T 2000 Single-molecule imaging of EGFR signalling on the surface of living cells *Nat. Cell Biol.* **2** 168–72

[26] Iino R, Koyama I and Kusumi A 2001 Single molecule imaging of green fluorescent proteins in living cells: E-cadherin forms oligomers on the free cell surface *Biophys. J.* **80** 2667–77

[27] Harms G S, Cognet L, Lommerse P H, Blab G A, Kahr H, Gamsjäger R, Spaink H P, Soldatov N M, Romanin C and Schmidt T 2001 Single-molecule imaging of L-type Ca^{2+} channels in live cells *Biophys. J.* **81** 2639–46

[28] Schmidt T, Schütz G, Baumgartner W, Gruber H and Schindler H 1996 Imaging of single molecule diffusion *Proc. Natl Acad. Sci.* **93** 2926–9

[29] Schütz G J, Kada G, Pastushenko V P and Schindler H 2000 Properties of lipid microdomains in a muscle cell membrane visualized by single molecule microscopy *EMBO J.* **19** 892–901

[30] Alcor D, Gouzer G and Triller A 2009 Single-particle tracking methods for the study of membrane receptors dynamics *Eur. J. Neurosci.* **30** 987–97

[31] Pinaud F, Clarke S, Sittner A and Dahan M 2010 Probing cellular events, one quantum dot at a time *Nat. Methods* **7** 275–85

[32] Kusumi A, Tsunoyama T A, Hirosawa K M, Kasai R S and Fujiwara T K 2014 Tracking single molecules at work in living cells *Nat. Chem. Biol.* **10** 524–32

[33] Elf J, Li G-W and Xie X S 2007 Probing transcription factor dynamics at the single-molecule level in a living cell *Science* **316** 1191–4

[34] Gebhardt J C M, Suter D M, Roy R, Zhao Z W, Chapman A R, Basu S, Maniatis T and Xie X S 2013 Single-molecule imaging of transcription factor binding to DNA in live mammalian cells *Nat. Methods* **10** 421–6

[35] Courty S, Luccardini C, Bellaiche Y, Cappello G and Dahan M 2006 Tracking individual kinesin motors in living cells using single quantum-dot imaging *Nano Lett.* **6** 1491–5

[36] Levi V and Gratton E 2009 Three-dimensional particle tracking in a laser scanning Fluorescence microscope *Single Particle Tracking and Single Molecule Energy Transfer* ed C Bräuchle *et al* (New York: Wiley) pp 3–24 ch 1

[37] Kubitscheck U, Veith R, Ritter J G and Siebrasse J P 2009 Messenger RNA trafficking in living cells *Single Particle Tracking and Single Molecule Energy Transfer* ed C Bräuchle *et al* (New York: Wiley) pp 43–66 ch 3

[38] Kusumi A, Nakada C, Ritchie K, Murase K, Suzuki K, Murakoshi H, Kasai R S, Kondo J and Fujiwara T 2005 Paradigm shift of the plasma membrane concept from the 2D continuum fluid to the partitioned fluid: high-speed single-molecule tracking of membrane molecules *Annu. Rev. Biophys. Biomol. Struct.* **34** 351–78

[39] Ortega-Arroyo J and Kukura P 2012 Interferometric scattering microscopy (iSCAT): new frontiers in ultrafast and ultrasensitive optical microscopy *Phys. Chem. Chem. Phys.* **14** 15625–36

[40] Dahan M, Levi S, Luccardini C, Rostaing P, Riveau B and Triller A 2003 Diffusion dynamics of glycine receptors revealed by single-quantum dot tracking *Science* **302** 442–5

[41] Cognet L, Leduc C and Lounis B 2014 Advances in live-cell single-particle tracking and dynamic super-resolution imaging *Curr. Opin. Chem. Biol.* **20** 78–85

[42] Kusumi A, Fujiwara T K, Chadda R, Xie M, Tsunoyama T A, Kalay Z, Kasai R S and Suzuki K G 2012 Dynamic organizing principles of the plasma membrane that regulate signal transduction: commemorating the fortieth anniversary of Singer and Nicolson's fluid-mosaic model *Annu. Rev. Cell Dev. Biol.* **28** 215–50

[43] Brandenburg B and Zhuang X 2007 Virus trafficking-learning from single-virus tracking *Nat. Rev. Microbiol.* **5** 197–208

[44] Dahan M, Alivisatos A P and Parak W J 2009 Quantum dots: inorganic Fluroscent probes for single-molecule tracking experiments in live cells *Single Particle Tracking and Single Molecule Energy Transfer* ed C Bräuchle *et al* (New York: Wiley) pp 67–96 ch 4

[45] Biermann B, Sokoll S, Klueva J, Missler M, Wiegert J S, Sibarita J B and Heine M 2014 Imaging of molecular surface dynamics in brain slices using single-particle tracking *Nat. Commun.* **5** 3024

[46] Höfling F and Franosch T 2013 Anomalous transport in the crowded world of biological cells *Rep. Prog. Phys.* **76** 046602

[47] Metzler R, Jeon J-H, Cherstvy A G and Barkai E 2014 Anomalous diffusion models and their properties: non-stationarity, non-ergodicity, and ageing at the centenary of single particle tracking *Phys. Chem. Chem. Phys.* **16** 24128–64

[48] Barkai E, Garini Y and Metzler R 2012 Strange kinetics of single molecules in living cells *Phys. Today* **65** 29

[49] Burov S, Jeon J-H, Metzler R and Barkai E 2011 Single particle tracking in systems showing anomalous diffusion: the role of weak ergodicity breaking *Phys. Chem. Chem. Phys.* **13** 1800–12

[50] Weigel A V, Simon B, Tamkun M M and Krapf D 2011 Ergodic and nonergodic processes coexist in the plasma membrane as observed by single-molecule tracking *Proc. Natl Acad. Sci. USA* **108** 6438–43

[51] Tabei S M A, Burov S, Kim H Y, Kuznetsov A, Huynh T, Jureller J, Philipson L H, Dinner A R and Scherer N F 2013 Intracellular transport of insulin granules is a subordinated random walk. *Proc. Natl Acad. Sci. USA* **110** 4911–6

[52] Jeon J-H, Tejedor V, Burov S, Barkai E, Selhuber-Unkel C, Berg-Sørensen K, Oddershede L and Metzler R 2011 *In vivo* anomalous diffusion and weak ergodicity breaking of lipid granules *Phys. Rev. Lett.* **106** 048103

[53] Manzo C, Torreno-Pina J A, Massignan P, Lapeyre Jr G J, Lewenstein M and Garcia-Parajo M F 2015 Weak ergodicity breaking of receptor motion in living cells stemming from random diffusivity *Phys. Rev. X* **5** 011021

[54] Tsien R Y 1998 The green fluorescent protein *Annu. Rev. Biochem.* **67** 509–44

[55] Clausen M P and Christoffer Lagerholm B 2011 The probe rules in single particle tracking *Curr. Protein Pept. Sci.* **12** 699–713

[56] Chen I and Ting A Y 2005 Site-specific labeling of proteins with small molecules in live cells *Curr. Opin. Biotechnol.* **16** 35–40

[57] Dempsey G T, Vaughan J C, Chen K H, Bates M and Zhuang X 2011 Evaluation of fluorophores for optimal performance in localization-based super-resolution imaging *Nat. Methods* **8** 1027–36

[58] Cognet L, Harms G S, Blab G A, Lommerse P H and Schmidt T 2000 Simultaneous dual-color and dual-polarization imaging of single molecules *Appl. Phys. Lett.* **77** 4052–4

[59] Ruthardt N, Lamb D C and Bräuchle C 2011 Single-particle tracking as a quantitative microscopy-based approach to unravel cell entry mechanisms of viruses and pharmaceutical nanoparticles *Mol. Ther.: J. Am. Soc. Gene Ther.* **19** 1199–211

[60] Wang Y, Shyy J Y-J and Chien S 2008 Fluorescence proteins, live-cell imaging, and mechanobiology: seeing is believing *Annu. Rev. Biomed. Eng.* **10** 1–38

[61] Fernández-Suárez M and Ting A Y 2008 Fluorescent probes for super-resolution imaging in living cells *Nat. Rev. Mol. Cell Biol.* **9** 929–43

[62] Garcia-Parajo M, Segers-Nolten G, Veerman J-A, Greve J and Van Hulst N 2000 Real-time light-driven dynamics of the fluorescence emission in single green fluorescent protein molecules *Proc. Natl Acad. Sci.* **97** 7237–42

[63] Bruchez M, Moronne M, Gin P, Weiss S and Alivisatos A P 1998 Semiconductor nanocrystals as fluorescent biological labels *Science* **281** 2013–6

[64] Michalet X, Pinaud F F, Bentolila L A, Tsay J M, Doose S, Li J J, Sundaresan G, Wu A M, Gambhir S S and Weiss S 2005 Quantum dots for live cells, *in vivo* imaging, and diagnostics *Science* **307** 538–44

[65] Resch-Genger U, Grabolle M, Cavaliere-Jaricot S, Nitschke R and Nann T 2008 Quantum dots versus organic dyes as fluorescent labels *Nat. Methods* **5** 763–75

[66] Howarth M, Liu W, Puthenveetil S, Zheng Y, Marshall L F, Schmidt M M, Wittrup K D, Bawendi M G and Ting A Y 2008 Monovalent, reduced-size quantum dots for imaging receptors on living cells *Nat. Methods* **5** 397–9

[67] Arnspang E C, Brewer J R and Lagerholm B C 2012 Multi-color single particle tracking with quantum dots *PLoS One* **7** e48521

[68] Cutler P J, Malik M D, Liu S, Byars J M, Lidke D S and Lidke K A 2013 Multi-color quantum dot tracking using a high-speed hyperspectral line-scanning microscope *PLoS One* **8** e64320

[69] Nirmal M, Dabbousi B, Bawendi M, Macklin J, Trautman J, Harris T and Brus L 1996 Fluorescence intermittency in single cadmium selenide nanocrystals *Nature* **383** 802–4

[70] Kuno M, Fromm D, Hamann H, Gallagher A and Nesbitt D 2000 Nonexponential 'blinking' kinetics of single CdSe quantum dots: a universal power law behavior *J. Chem. Phys.* **112** 3117–20

[71] Margolin G, Protasenko V, Kuno M and Barkai E 2006 Power law blinking quantum dots: Stochastic and physical models *Fractals, Diffusion and Relaxation in Disordered Complex Systems: Advances in Chemical Physics*, ed W T Coffey and Y P Halmykov Hoboken (New York: Wiley) ch 4

[72] Mahler B, Spinicelli P, Buil S, Quelin X, Hermier J-P and Dubertret B 2008 Towards non-blinking colloidal quantum dots *Nat. Mater.* **7** 659–64

[73] Wang X, Ren X, Kahen K, Hahn M A, Rajeswaran M, Maccagnano-Zacher S, Silcox J, Cragg G E, Efros A L and Krauss T D 2009 Non-blinking semiconductor nanocrystals *Nature* **459** 686–9

[74] Sergé A, Bertaux N, Rigneault H and Marguet D 2008 Dynamic multiple-target tracing to probe spatiotemporal cartography of cell membranes *Nat. Methods* **5** 687–94

[75] Wieser S and Schütz G J 2008 Tracking single molecules in the live cell plasma membrane—do's and don't's *Methods* **46** 131–40

[76] Tokunaga M, Imamoto N and Sakata-Sogawa K 2008 Highly inclined thin illumination enables clear single-molecule imaging in cells *Nat. Methods* **5** 159–61

[77] Ritter J G, Veith R, Veenendaal A, Siebrasse J P and Kubitscheck U 2010 Light sheet microscopy for single molecule tracking in living tissue *PLoS One* **5** e11639

[78] Friedrich M, Nozadze R, Gan Q, Zelman-Femiak M, Ermolayev V, Wagner T U and Harms G S 2009 Detection of single quantum dots in model organisms with sheet illumination microscopy *Biochem. Biophys. Res. Commun.* **390** 722–7

[79] Axelrod D 2001 Total internal reflection fluorescence microscopy in cell biology *Traffic* **2** 764–74

[80] Wazawa T and Ueda M 2005 Total internal reflection fluorescence microscopy in single molecule nanobioscience *Microscopy Techniques* ed J Rietdorf (Berlin: Springer) ch 4 pp 77–106

[81] Spille J-H 2013 Three dimensional single particle tracking in a light sheet microscope *PhD Thesis* Rheinischen Friedrich-Wilhelms-Universität Bonn

[82] Huisken J, Swoger J, Del Bene F, Wittbrodt J and Stelzer E H 2004 Optical sectioning deep inside live embryos by selective plane illumination microscopy *Science* **305** 1007–9

[83] Keller P J, Schmidt A D, Wittbrodt J and Stelzer E H 2008 Reconstruction of zebrafish early embryonic development by scanned light sheet microscopy *Science* **322** 1065–9

[84] Weber M and Huisken J 2011 Light sheet microscopy for real-time developmental biology *Curr. Opin. Genet. Dev.* **21** 566–72

[85] Arhel N, Genovesio A, Kim K-A, Miko S, Perret E, Olivo-Marin J-C, Shorte S and Charneau P 2006 Quantitative 4D tracking of cytoplasmic and nuclear HIV-1 complexes *Nat. Methods* **3** 817–24

[86] Lange S, Katayama Y, Schmid M, Burkacky O, Bräuchle C, Lamb D C and Jansen R P 2008 Simultaneous transport of different localized mRNA species revealed by live-cell imaging *Traffic* **9** 1256–67

[87] Izquierdo-Useros N, Esteban O, Rodriguez-Plata M T, Erkizia I, Prado J G, Blanco J, García-Parajo M F and Martinez-Picado J 2011 Dynamic imaging of cell-free and cell-associated viral capture in mature dendritic cells *Traffic* **12** 1702–13

[88] Manley S, Gillette J M, Patterson G H, Shroff H, Hess H F, Betzig E and Lippincott-Schwartz J 2008 High-density mapping of single-molecule trajectories with photoactivated localization microscopy *Nat. Methods* **5** 155–7

[89] Rossier O, Octeau V, Sibarita J-B, Leduc C, Tessier B, Nair D, Gatterdam V, Destaing O, Albiges-Rizo C and Tampé R 2012 Integrins β1 and β3 exhibit distinct dynamic nanoscale organizations inside focal adhesions *Nat. Cell Biol.* **14** 1057–67

[90] Paszek M J, DuFort C C, Rossier O, Bainer R, Mouw J K, Godula K, Hudak J E, Lakins J N, Wijekoon A C and Cassereau L 2014 The cancer glycocalyx mechanically primes integrin-mediated growth and survival *Nature* **511** 319–25

[91] Giannone G, Hosy E, Levet F, Constals A, Schulze K, Sobolevsky A I, Rosconi M P, Gouaux E, Tampé R and Choquet D 2010 Dynamic superresolution imaging of endogenous proteins on living cells at ultra-high density *Biophys. J.* **99** 1303–10

[92] Benke A, Olivier N, Gunzenhäuser J and Manley S 2012 Multicolor single molecule tracking of stochastically active synthetic dyes *Nano Lett.* **12** 2619–24

[93] Appelhans T, Richter C P, Wilkens V, Hess S T, Piehler J and Busch K B 2012 Nanoscale organization of mitochondrial microcompartments revealed by combining tracking and localization microscopy *Nano Lett.* **12** 610–6

[94] Schütz G J, Axmann M and Schindler H 2001 Imaging single molecules in 3D *Single Mol.* **2** 69–74

[95] Levi V, Ruan Q and Gratton E 2005 3D particle tracking in a two-photon microscope: application to the study of molecular dynamics in cells *Biophys. J.* **88** 2919–28

[96] Levi V and Gratton E 2007 Exploring dynamics in living cells by tracking single particles *Cell Biochem. Biophys.* **48** 1–15

[97] Levi V, Ruan Q, Plutz M, Belmont A S and Gratton E 2005 Chromatin dynamics in interphase cells revealed by tracking in a two-photon excitation microscope *Biophys. J.* **89** 4275–85

[98] Speidel M, Jonáš A and Florin E-L 2003 3D tracking of fluorescent nanoparticles with subnanometer precision by use of off-focus imaging *Opt. Lett.* **28** 69–71

[99] Toprak E, Balci H, Blehm B H and Selvin P R 2007 3D particle tracking via bifocal imaging *Nano Lett.* **7** 2043–5

[100] Mlodzianoski M J, Juette M F, Beane G L and Bewersdorf J 2009 Experimental characterization of 3D localization techniques for particle-tracking and super-resolution microscopy *Opt. Express* **17** 8264–77

[101] Thompson M A, Casolari J M, Badieirostami M, Brown P O and Moerner W 2010 3D tracking of single mRNA particles in *Saccharomyces cerevisiae* using a double-helix point spread function *Proc. Natl Acad. Sci.* **107** 17864–71

[102] Holtzer L, Meckel T and Schmidt T 2007 Nanometric 3D tracking of individual quantum dots in cells *Appl. Phys. Lett.* **90** 053902

[103] Kao H P and Verkman A 1994 Tracking of single fluorescent particles in 3D: use of cylindrical optics to encode particle position *Biophys. J.* **67** 1291

[104] Kapanidis A N, Laurence T A, Lee N K, Margeat E, Kong X and Weiss S 2005 Alternating-laser excitation of single molecules *Acc. Chem. Res.* **38** 523–33

[105] Boyer D, Tamarat P, Maali A, Lounis B and Orrit M 2002 Photothermal imaging of nanometer-sized metal particles among scatterers *Science* **297** 1160–3

[106] Cognet L, Tardin C, Boyer D, Choquet D, Tamarat P and Lounis B 2003 Single metallic nanoparticle imaging for protein detection in cells *Proc. Natl Acad. Sci.* **100** 11350–5

[107] Lasne D, Blab G A, Berciaud S, Heine M, Groc L, Choquet D, Cognet L and Lounis B 2006 Single nanoparticle photothermal tracking (SNaPT) of 5 nm gold beads in live cells *Biophys. J.* **91** 4598–604

[108] Leduc C, Si S, Gautier J, Soto-Ribeiro M, Wehrle-Haller B, Gautreau A, Giannone G, Cognet L and Lounis B 2013 A highly specific gold nanoprobe for live-cell single-molecule imaging *Nano Lett.* **13** 1489–94

[109] Kukura P, Ewers H, Müller C, Renn A, Helenius A and Sandoghdar V 2009 High-speed nanoscopic tracking of the position and orientation of a single virus *Nat. Methods* **6** 923–7

[110] Piliarik M and Sandoghdar V 2014 Direct optical sensing of single unlabelled proteins and super-resolution imaging of their binding sites *Nat. Commun.* **5** 4495

[111] Spillane K M, Ortega-Arroyo J, de Wit G, Eggeling C, Ewers H, Wallace M I and Kukura P 2014 High-speed single-particle tracking of GM1 in model membranes reveals anomalous diffusion due to interleaflet coupling and molecular pinning *Nano Lett.* **14** 5390–7

[112] Ortega Arroyo J, Andrecka J, Spillane K M, Billington N, Takagi Y, Sellers J R and Kukura P 2014 Label-free, all-optical detection, imaging, and tracking of a single protein *Nano Lett.* **14** 2065–70

[113] Small A and Stahlheber S 2014 Fluorophore localization algorithms for super-resolution microscopy *Nat. Methods* **11** 267–79

[114] Deschout H, Zanacchi F C, Mlodzianoski M, Diaspro A, Bewersdorf J, Hess S T and Braeckmans K 2014 Precisely and accurately localizing single emitters in fluorescence microscopy *Nat. Methods* **11** 253–66

[115] Saxton M J 2008 Single-particle tracking: connecting the dots *Nat. Methods* **5** 671–2

[116] Saxton M J 2014 A particle tracking meet *Nat. Methods* **11** 247–8

[117] Thompson R E, Larson D R and Webb W W 2002 Precise nanometer localization analysis for individual fluorescent probes *Biophys. J.* **82** 2775–83

[118] Abraham A V, Ram S, Chao J, Ward E S and Ober R J 2009 Quantitative study of single molecule location estimation techniques *Opt. Express* **17** 23352–73

[119] Ober R J, Ram S and Ward E S 2004 Localization accuracy in single-molecule microscopy *Biophys. J.* **86** 1185–200

[120] Deschout H, Neyts K and Braeckmans K 2012 The influence of movement on the localization precision of sub-resolution particles in fluorescence microscopy *J. Biophoton.* **5** 97–109

[121] Wong Y, Lin Z and Ober R J 2011 Limit of the accuracy of parameter estimation for moving single molecules imaged by fluorescence microscopy *IEEE Trans. Signal Process.* **59** 895–911

[122] Betzig E, Patterson G H, Sougrat R, Lindwasser O W, Olenych S, Bonifacino J S, Davidson M W, Lippincott-Schwartz J and Hess H F 2006 Imaging intracellular fluorescent proteins at nanometer resolution *Science* **313** 1642–5

[123] Rust M J, Bates M and Zhuang X 2006 Sub-diffraction-limit imaging by stochastic optical reconstruction microscopy (STORM) *Nat. Methods* **3** 793–6

[124] Yildiz A and Selvin P R 2005 Fluorescence imaging with one nanometer accuracy: application to molecular motors *Acc. Chem. Res.* **38** 574–82

[125] Engelhardt J, Keller J, Hoyer P, Reuss M, Staudt T and Hell S W 2011 Molecular orientation affects localization accuracy in superresolution far-field fluorescence microscopy *Nano Lett.* **11** 209–13

[126] Enderlein J 2000 Theoretical study of detection of a dipole emitter through an objective with high numerical aperture *Opt. Lett.* **25** 634–6

[127] Stallinga S and Rieger B 2010 Accuracy of the Gaussian point spread function model in 2D localization microscopy *Opt. Express* **18** 24461–76

[128] Stallinga S and Rieger B 2012 Position and orientation estimation of fixed dipole emitters using an effective Hermite point spread function model *Opt. Express* **20** 5896–921

[129] Aguet F, Geissbuhler S, Marki I, Lasser T and Unser M 2009 Super-resolution orientation estimation and localization of fluorescent dipoles using 3D steerable filters *Opt. Express* **17** 6829–48

[130] Godinez W J, Lampe M, Eils R, Muller B and Rohr K 2011 Tracking multiple particles in fluorescence microscopy images via probabilistic data association *Biomedical Imaging: From Nano to Micro, 2011 IEEE Int. Symp. on* pp 1925–8

[131] Parthasarathy R 2012 Rapid, accurate particle tracking by calculation of radial symmetry centers *Nat. Methods* **9** 724–6

[132] Richards B and Wolf E 1959 Electromagnetic diffraction in optical systems: II. Structure of the image field in an aplanatic system *Proc. R. Soc.* A **253** 358–79

[133] Gibson S F and Lanni F 1992 Experimental test of an analytical model of aberration in an oil-immersion objective lens used in 3D light microscopy *J. Opt. Soc. Am.* A **9** 154–66

[134] Zhang B, Zerubia J and Olivo-Marin J-C 2007 Gaussian approximations of fluorescence microscope point-spread function models *Appl. Opt.* **46** 1819–29

[135] Huang F *et al* 2013 Video-rate nanoscopy using sCMOS camera-specific single-molecule localization algorithms *Nat. Methods* **10** 653–8

[136] Quan T, Zeng S and Huang Z-L 2010 Localization capability and limitation of electron-multiplying charge-coupled, scientific complementary metal-oxide semiconductor, and charge-coupled devices for superresolution imaging *J. Biomed. Opt.* **15** 066005

[137] Chao J, Ram S, Ward E S and Ober R J 2013 Ultrahigh accuracy imaging modality for super-localization microscopy *Nat. Methods* **10** 335–8

[138] Cheezum M K, Walker W F and Guilford W H 2001 Quantitative comparison of algorithms for tracking single fluorescent particles *Biophys. J.* **81** 2378–88

[139] Smith C S, Joseph N, Rieger B and Lidke K A 2010 Fast, single-molecule localization that achieves theoretically minimum uncertainty *Nat. Methods* **7** 373–5

[140] Mortensen K I, Churchman L S, Spudich J A and Flyvbjerg H 2010 Optimized localization analysis for single-molecule tracking and super-resolution microscopy *Nat. Methods* **7** 377–81

[141] Henriques R, Lelek M, Fornasiero E F, Valtorta F, Zimmer C and Mhlanga M M 2010 QuickPALM: 3D real-time photoactivation nanoscopy image processing in Image *J. Nat. Methods* **7** 339–40

[142] Berglund A J, McMahon M D, McClelland J J and Liddle J A 2008 Fast, bias-free algorithm for trackingsingle particles with variable size and shape *Opt. Express* **16** 14064–75

[143] Andersson S 2008 Localization of a fluorescent source without numerical fitting *Opt. Express* **16** 18714–24

[144] Hedde P N, Fuchs J, Oswald F, Wiedenmann J and Nienhaus G U 2009 Online image analysis software for photoactivation localization microscopy *Nat. Methods* **6** 689–90

[145] Yu B, Chen D, Qu J and Niu H 2011 Fast Fourier domain localization algorithm of a single molecule with nanometer precision *Opt. Lett.* **36** 4317–9

[146] Sbalzarini I F and Koumoutsakos P 2005 Feature point tracking and trajectory analysis for video imaging in cell biology *J. Struct. Biol.* **151** 182–95

[147] Olivo-Marin J C 2002 Extraction of spots in biological images using multiscale products *Pattern Recognit.* **35** 1989–96

[148] Godinez W J 2009 Deterministic and probabilistic approaches for tracking virus particles in time-lapse fluorescence microscopy image sequences *Med. Image Anal.* **13** 325–42

[149] Rink J, Ghigo E, Kalaidzidis Y and Zerial M 2005 Rab conversion as a mechanism of progression from early to late endosomes *Cell* **122** 735–49

[150] Liang L, Shen H, De Camilli P and Duncan J S 2010 Tracking clathrin coated pits with a multiple hypothesis based method *Med. Image Comput. Comput. Assist. Interv.* **6362** 315–22

[151] Yin Z, Kanade T and Chen M 2012 Understanding the phase contrast optics to restore artifact-free microscopy images for segmentation *Med. Image Anal.* **16** 1047–62

[152] Lowe D G 2004 Distinctive image features from scale-invariant keypoints *Int. J. Comput. Vis.* **60** 91–110

[153] Celler K, van Wezel G P and Willemse J 2013 Single particle tracking of dynamically localizing TatA complexes in *Streptomyces coelicolor Biochem. Biophys. Res. Commun.* **438** 38–42

[154] Crocker J C and Grier D G 1996 Methods of digital video microscopy for colloidal studies *J. Colloid Interface Sci.* **179** 298–310

[155] Ku T C 2007 An automated tracking system to measure the dynamic properties of vesicles in living cells *Microsc. Res. Tech.* **70** 119–34

[156] Ku T C, Kao L S, Lin C C and Tsai Y S 2009 Morphological filter improve the efficiency of automated tracking of secretory vesicles with various dynamic properties *Microsc. Res. Tech.* **72** 639–49

[157] Quan T 2011 High-density localization of active molecules using structured sparse model and Bayesian information criterion *Opt. Express* **19** 16963–74

[158] Wang Y, Quan T, Zeng S and Huang Z L 2012 PALMER: a method capable of parallel localization of multiple emitters for high-density localization microscopy *Opt. Express* **20** 16039–49

[159] Ram S, Ward E S and Ober R J 2006 Beyond Rayleigh's criterion: a resolution measure with application to single-molecule microscopy *Proc. Natl Acad. Sci. USA* **103** 4457–62

[160] Manzo C, van Zanten T S, Saha S, Torreno-Pina J A, Mayor S and Garcia-Parajo M F 2014 PSF decomposition of nanoscopy images via Bayesian analysis unravels distinct molecular organization of the cell membrane *Sci. Rep.* **4** 4354

[161] Holden S J, Uphoff S and Kapanidis A N 2011 DAOSTORM: an algorithm for high- density super-resolution microscopy *Nat. Methods* **8** 279–80

[162] Zhu L, Zhang W, Elnatan D and Huang B 2012 Faster STORM using compressed sensing *Nat. Methods* **9** 721–3

[163] Shafique K and Shah M 2005 A noniterative greedy algorithm for multiframe point correspondence *IEEE Trans. Pattern Anal. Mach. Intell.* **27** 51–65

[164] Jaqaman K 2008 Robust single-particle tracking in live-cell time-lapse sequences *Nat. Methods* **5** 695–702

[165] Coraluppi S and Carthel C 2004 Recursive track fusion for multi-sensor surveillance *Inf. Fusion* **5** 23–33

[166] Coraluppi S and Carthel C 2011 Multi-stage multiple-hypothesis tracking *J. Adv. Inf. Fusion* **6** 57–67

[167] Chenouard N, Bloch I and Olivo-Marin J C 2009 Multiple hypothesis tracking in cluttered condition *16th IEEE Int. Conf. on Image Processing* pp 3621–4

[168] Chenouard N, Bloch I and Olivo-Marin J C 2009 Multiple hypothesis tracking in microscopy images *Biomedical Imaging: From Nano to Macro Proc. IEEE Int. Symp.* pp 1346–9

[169] Winter M 2011 Vertebrate neural stem cell segmentation, tracking and lineaging with validation and editing *Nat. Protocols* **6** 1942–52

[170] Winter M R, Fang C, Banker G, Roysam B and Cohen A R 2012 Axonal transport analysis using multitemporal association tracking *Int. J. Comput. Biol. Drug Des.* **5** 35–48

[171] Verestóy J, Csetverikov D and Nagy M 1999 Digital particle image velocimetry: a challenge for feature based tracking *Mach. Graph. Vis.* **8** 553–69

[172] Poore A B and Gadaleta S 2006 Some assignment problems arising from multiple target tracking *Math. Comput. Modelling* **43** 1074–91

[173] Magnusson K E G and Jalden J 2012 A batch algorithm using iterative application of the Viterbi algorithm to track cells and construct cell lineages *Biomedical Imaging Proc. IEEE Int. Symp.* pp 382–5

[174] Racine V, Hertzog A, Jouanneau J, Salamero J, Kervrann C and Sibarita J B 2006 *Biomedical Imaging: Nano to Macro 3rd IEEE Int. Symp.* pp 1020–3

[175] Krapf D 2015 Mechanisms underlying anomalous diffusion is the plasma membrane *Current Topics in Membranes* ed A K Henworthy (New York: Academic) pp 167–207

[176] Bálint Š, Vilanova I V, Álvarez Á S and Lakadamyali M 2013 Correlative live-cell and superresolution microscopy reveals cargo transport dynamics at microtubule intersections *Proc. Natl Acad. Sci.* **110** 3375–80

[177] Kusumi A, Sako Y and Yamamoto M 1993 Confined lateral diffusion of membrane receptors as studied by single particle tracking (nanovid microscopy). Effects of calcium-induced differentiation in cultured epithelial cells *Biophys. J.* **65** 2021–40

[178] Destainville N and Salomé L 2006 Quantification and correction of systematic errors due to detector time-averaging in single-molecule tracking experiments *Biophys. J.* **90** L17–9

[179] Saxton M J 1995 Single-particle tracking: effects of corrals *Biophys. J.* **69** 389–98

[180] Michalet X 2010 Mean square displacement analysis of single-particle trajectories with localization error: Brownian motion in an isotropic medium *Phys. Rev.* E **82** 041914

[181] Kepten E, Weron A, Sikora G, Burnecki K and Garini Y 2015 Guidelines for the fitting of anomalous diffusion mean square displacement graphs from single particle tracking experiments *PLoS One* **10** e0117722

[182] Martin D S, Forstner M B and Käs J A 2002 Apparent subdiffusion inherent to single particle tracking *Biophys. J.* **83** 2109–17

[183] Berglund A J 2010 Statistics of camera-based single-particle tracking *Phys. Rev.* E **82** 1–8

[184] Michalet X and Berglund A J 2012 Optimal diffusion coefficient estimation in single-particle tracking *Phys. Rev.* E **85** 061916

[185] Burnecki K, Kepten E, Garini Y, Sikora G and Weron A 2015 Estimating the anomalous diffusion exponent for single particle tracking data with measurement errors-An alternative approach *Sci. Rep.* **5** 11306

[186] Qian H, Sheetz M P and Elson E L 1991 Single particle tracking. Analysis of diffusion and flow in 2D systems *Biophys. J.* **60** 910–21

[187] Schütz G J, Schindler H and Schmidt T 1997 Single-molecule microscopy on model membranes reveals anomalous diffusion *Biophys. J.* **73** 1073–80

[188] Pinaud F, Michalet X, Iyer G, Margeat E, Moore H-P and Weiss S 2009 Dynamic partitioning of a glycosyl-phosphatidylinositol-anchored protein in glycosphingolipid-rich microdomains imaged by single-quantum dot tracking *Traffic* **10** 691–712

[189] Ferrari R, Manfroi A J and Young W R 2001 Strongly and weakly self-similar diffusion *Physica* D **154** 111–37

[190] Ewers H, Smith A E, Sbalzarini I F, Lilie H, Koumoutsakos P and Helenius A 2005 Single-particle tracking of murine polyoma virus-like particles on live cells and artificial membranes *Proc. Natl Acad. Sci. USA* **102** 15110–5
[191] Türkcan S and Masson J-B 2013 Bayesian decision tree for the classification of the mode of motion in single-molecule trajectories *PLoS One* **8** e82799
[192] Voisinne G, Alexandrou A and Masson J-B 2010 Quantifying biomolecule diffusivity using an optimal Bayesian method *Biophys. J.* **98** 596–605
[193] Türkcan S, Alexandrou A and Masson J B 2012 A Bayesian inference scheme to extract diffusivity and potential fields from confined single-molecule trajectories *Biophys. J.* **102** 2288–98
[194] Burov S, Tabei S M A, Huynh T, Murrell M P, Philipson L H, Rice S A, Gardel M L, Scherer N F and Dinner A R 2013 Distribution of directional change as a signature of complex dynamics *Proc. Natl Acad. Sci. USA* **110** 19689–94
[195] Tejedor V, Bénichou O, Voituriez R, Jungmann R, Simmel F, Selhuber-Unkel C, Oddershede L B and Metzler R 2010 Quantitative analysis of single particle trajectories: Mean maximal excursion method *Biophys. J.* **98** 1364–72
[196] Huet S, Karatekin E, Tran V S, Fanget I, Cribier S and Henry J-P 2006 Analysis of transient behavior in complex trajectories: application to secretory vesicle dynamics *Biophys. J.* **91** 3542–59
[197] Simson R, Sheets E D and Jacobson K 1995 Detection of temporary lateral confinement of membrane proteins using single-particle tracking analysis *Biophys. J.* **69** 989–93
[198] Helmuth J A, Burckhardt C J, Koumoutsakos P, Greber U F and Sbalzarini I F 2007 A novel supervised trajectory segmentation algorithm identifies distinct types of human adenovirus motion in host cells *J. Struct. Biol.* **159** 347–58
[199] Montiel D, Cang H and Yang H 2006 Quantitative characterization of changes in dynamical behavior for single-particle tracking studies *J. Phys. Chem.* B **110** 19763–70
[200] Bosch P J, Kanger J S and Subramaniam V 2014 Classification of dynamical diffusion states in single molecule tracking microscopy *Biophys. J.* **107** 588–98
[201] Low-Nam S T, Lidke K A, Cutler P J, Roovers R C, van Bergen en Henegouwen P M P, Wilson B S and Lidke D S 2011 ErbB1 dimerization is promoted by domain co-confinement and stabilized by ligand binding *Nat. Struct. Mol. Biol.* **18** 1244–9
[202] Masson J-B, Dionne P, Salvatico C, Renner M, Specht C G, Triller A and Dahan M 2014 Mapping the energy and diffusion landscapes of membrane proteins at the cell surface using high-density single-molecule imaging and Bayesian inference: application to the multiscale dynamics of glycine receptors in the neuronal membrane *Biophys. J.* **106** 74–83
[203] Torreno-Pina J A, Castro B M, Manzo C, Buschow S I, Cambi A and Garcia-Parajo M F 2014 Enhanced receptor–clathrin interactions induced by N-glycan-mediated membrane micropatterning *Proc. Natl. Acad. Sci. USA* **111** 11037–42
[204] Li H, Dou S-X, Liu Y-R, Li W, Xie P, Wang W-C and Wang P-Y 2015 Mapping intracellular diffusion distribution using single quantum dot tracking: compartmentalized diffusion defined by endoplasmic reticulum *J. Am. Chem. Soc.* **137** 436–44
[205] Singer S and Nicolson G L 1972 The fluid mosaic model of the structure of cell membranes *Membranes and Viruses in Immunopathology* ed S B Day and R A Good (New York: Academic) pp 7–47
[206] Kusumi A, Suzuki K G, Kasai R S, Ritchie K and Fujiwara T K 2011 Hierarchical mesoscale domain organization of the plasma membrane *Trends Biochem. Sci.* **36** 604–15
[207] Maxfield F R 2002 Plasma membrane microdomains *Curr. Opin. Cell Biol.* **14** 483–7
[208] Nicolson G L 2013 Update of the 1972 Singer–Nicolson fluid-mosaic model of membrane structure *Discoveries* **1** e3
[209] van Zanten T S, Cambi A and Garcia-Parajo M F 2010 A nanometer scale optical view on the compartmentalization of cell membranes *Biochim. Biophys. Acta (BBA)-Biomembr.* **1798** 777–87
[210] Garcia-Parajo M F, Cambi A, Torreno-Pina J A, Thompson N and Jacobson K 2014 Nanoclustering as a dominant feature of plasma membrane organization *J. Cell Sci.* **127** 4995–5005
[211] Klotzsch E and Schütz G J 2013 A critical survey of methods to detect plasma membrane rafts *Phil. Trans. R. Soc.* B **368** 20120033
[212] Lingwood D and Simons K 2010 Lipid rafts as a membrane-organizing principle *Science* **327** 46–50
[213] Griffié J, Burn G and Owen D M The nanoscale organisation of signaling domains at the plasma membrane *Current Topics in Membranes* ed A K Kenworthy (New York: Academic) pp 125–65
[214] Suzuki K G, Kasai R S, Hirosawa K M, Nemoto Y L, Ishibashi M, Miwa Y, Fujiwara T K and Kusumi A 2012 Transient GPI-anchored protein homodimers are units for raft organization and function *Nat. Chem. Biol.* **8** 774–83
[215] Gowrishankar K, Ghosh S, Saha S, Rumamol C, Mayor S and Rao M 2012 Active remodeling of cortical actin regulates spatiotemporal organization of cell surface molecules *Cell* **149** 1353–67
[216] Chaudhuri A, Bhattacharya B, Gowrishankar K, Mayor S and Rao M 2011 Spatiotemporal regulation of chemical reactions by active cytoskeletal remodeling *Proc. Natl Acad. Sci.* **108** 14825–30
[217] Sheetz M 1983 Membrane skeletal dynamics: role in modulation of red cell deformability, mobility of transmembrane proteins, and shape *Semin. Hematol.* **20** 175–88
[218] Owen D M, Williamson D, Rentero C and Gaus K 2009 Quantitative microscopy: protein dynamics and membrane organisation *Traffic* **10** 962–71
[219] Suzuki K G, Fujiwara T K, Sanematsu F, Iino R, Edidin M and Kusumi A 2007 GPI-anchored receptor clusters transiently recruit Lyn and Gα for temporary cluster immobilization and Lyn activation: single-molecule tracking study 1 *J. Cell biol.* **177** 717–30
[220] Suzuki K G, Fujiwara T K, Edidin M and Kusumi A 2007 Dynamic recruitment of phospholipase Cγ at transiently immobilized GPI-anchored receptor clusters induces IP3–Ca^{2+} signaling: single-molecule tracking study 2 *J. Cell Biol.* **177** 731–42
[221] Andrews N L, Lidke K A, Pfeiffer J R, Burns A R, Wilson B S, Oliver J M and Lidke D S 2008 Actin restricts Fcε RI diffusion and facilitates antigen-induced receptor immobilization *Nat. Cell Biol.* **10** 955–63
[222] Goswami D, Gowrishankar K, Bilgrami S, Ghosh S, Raghupathy R, Chadda R, Vishwakarma R, Rao M and Mayor S 2008 Nanoclusters of GPI-anchored proteins are formed by cortical actin-driven activity *Cell* **135** 1085–97
[223] Treanor B, Depoil D, Gonzalez-Granja A, Barral P, Weber M, Dushek O, Bruckbauer A and Batista F D 2010 The membrane skeleton controls diffusion dynamics and signaling through the B cell receptor *Immunity* **32** 187–99
[224] Jaqaman K, Kuwata H, Touret N, Collins R, Trimble W S, Danuser G and Grinstein S 2011 Cytoskeletal control of CD36 diffusion promotes its receptor and signaling function *Cell* **146** 593–606

[225] Jaumouillé V, Farkash Y, Jaqaman K, Das R, Lowell C A and Grinstein S 2014 Actin cytoskeleton reorganization by Syk regulates Fc*γ* receptor responsiveness by increasing its lateral mobility and clustering *Dev. Cell* **29** 534–46

[226] Freeman S A, Jaumouillé V, Choi K, Hsu B E, Wong H S, Abraham L, Graves M L, Coombs D, Roskelley C D and Das R 2015 Toll-like receptor ligands sensitize B-cell receptor signalling by reducing actin-dependent spatial confinement of the receptor *Nat. Commun.* **6** 6168

[227] Espenel C, Margeat E, Dosset P, Arduise C, Le Grimellec C, Royer C A, Boucheix C, Rubinstein E and Milhiet P-E 2008 Single-molecule analysis of CD9 dynamics and partitioning reveals multiple modes of interaction in the tetraspanin web *J. Cell Biol.* **182** 765–76

[228] Weigel A V, Tamkun M M and Krapf D 2013 Quantifying the dynamic interactions between a clathrin-coated pit and cargo molecules *Proc. Natl Acad. Sci. USA* **110** E4591–600

[229] Bakker G J, Eich C, Torreno-Pina J A, Diez-Ahedo R, Perez-Samper G, van Zanten T S, Figdor C G, Cambi A and Garcia-Parajo M F 2012 Lateral mobility of individual integrin nanoclusters orchestrates the onset for leukocyte adhesion *Proc. Natl Acad. Sci.* **109** 4869–74

[230] Andrews N L, Pfeiffer J R, Martinez A M, Haaland D M, Davis R W, Kawakami T, Oliver J M, Wilson B S and Lidke D S 2009 Small, mobile FcεRI receptor aggregates are signaling competent *Immunity* **31** 469–79

[231] Groc L, Lafourcade M, Heine M, Renner M, Racine V, Sibarita J-B, Lounis B, Choquet D and Cognet L 2007 Surface trafficking of neurotransmitter receptor: comparison between single-molecule/quantum dot strategies *J. Neurosci.* **27** 12433–7

[232] Maglione M and Sigrist S J 2013 Seeing the forest tree by tree: super-resolution light microscopy meets the neurosciences *Nat. Neurosci.* **16** 790–7

[233] Lakadamyali M, Rust M J, Babcock H P and Zhuang X 2003 Visualizing infection of individual influenza viruses *Proc. Natl Acad. Sci.* **100** 9280–5

[234] Rust M J, Lakadamyali M, Zhang F and Zhuang X 2004 Assembly of endocytic machinery around individual influenza viruses during viral entry *Nat. Struct. Mol. Biol.* **11** 567–73

[235] Brandenburg B, Lee L Y, Lakadamyali M, Rust M J, Zhuang X and Hogle J M 2007 Imaging poliovirus entry in live cells *PLoS Biol.* **5** e183

[236] Lakadamyali M, Rust M J and Zhuang X 2006 Ligands for clathrin-mediated endocytosis are differentially sorted into distinct populations of early endosomes *Cell* **124** 997–1009

[237] Lidke D S, Lidke K A, Rieger B, Jovin T M and Arndt-Jovin D J 2005 Reaching out for signals filopodia sense EGF and respond by directed retrograde transport of activated receptors *J. Cell Biol.* **170** 619–26

[238] Lidke D S, Nagy P, Heintzmann R, Arndt-Jovin D J, Post J N, Grecco H E, Jares-Erijman E A and Jovin T M 2004 Quantum dot ligands provide new insights into erbB/HER receptor-mediated signal transduction *Nat. Biotechnol.* **22** 198–203

[239] Cui B, Wu C, Chen L, Ramirez A, Bearer E L, Li W-P, Mobley W C and Chu S 2007 One at a time, live tracking of NGF axonal transport using quantum dots *Proc. Natl Acad. Sci.* **104** 13666–71

[240] Rajan S S, Liu H Y and Vu T Q 2008 Ligand-bound quantum dot probes for studying the molecular scale dynamics of receptor endocytic trafficking in live cells *ACS Nano* **2** 1153–66

[241] Pierobon P, Achouri S, Courty S, Dunn A R, Spudich J A, Dahan M and Cappello G 2009 Velocity, processivity, and individual steps of single myosin V molecules in live cells *Biophys. J.* **96** 4268–75

[242] Nelson S R, Ali M Y, Trybus K M and Warshaw D M 2009 Random walk of processive, quantum dot-labeled myosin Va molecules within the actin cortex of COS-7 cells *Biophys. J.* **97** 509–18

[243] Handwerger K E and Gall J G 2006 Subnuclear organelles: new insights into form and function *Trends Cell Biol.* **16** 19–26

[244] Misteli T 2007 Beyond the sequence: cellular organization of genome function *Cell* **128** 787–800

[245] Levi V and Gratton E 2008 Chromatin dynamics during interphase explored by single-particle tracking *Chromosome Res.* **16** 439–49

[246] Izeddin I, Récamier V, Bosanac L, Cissé I I, Boudarene L, Dugast-Darzacq C, Proux F, Bénichou O, Voituriez R and Bensaude O 2014 Single-molecule tracking in live cells reveals distinct target-search strategies of transcription factors in the nucleus *Elife* **3** e02230

[247] Titus Lucretius Carus 2013 *De Rerum Natura (On the Nature of Things)* (London: Forgotten Books)

[248] Perrin J 1909 Brownian movement and molecular reality *Ann. Chim. Phys.* **18** 5–114

[249] Nordlund I 1914 New determination of the Avogadro constant from the Brownian motion of small spheres of mercury suspended in water *Z. Phys. Chem.* **87** 40–62

[250] Einstein A 1905 On the movement of small particles suspended in a stationary liquid demanded by the molecular-kinetic theory of heat *Ann. Phys., Lpz.* **17** 549–60

[251] Langevin P 1908 Sur la théorie du mouvement Brownien *C. R. Acad. Sci. Paris* **146** 530–3

[252] Brown R 1828 Mikroskopische Beobachtungen über die im Pollen der Pflanzen enthaltenen Partikeln, und über das allgemeine Vorkommen activer Molecüle in organischen und unorganischen Körpern *Ann. Phys., Lpz.* **90** 294–313

[253] Weiss M 2014 Crowding, diffusion and biochemical reactions *International Review of cell and Molecular Biology* **307** 383–417

[254] Klafter J and Sokolov I M 2011 *First Steps in Random Walks: from Tools to Applications* (Oxford: Oxford University Press)

[255] Pearson K 1905 The problem of the random walk *Nature* **72** 294

[256] von Smoluchowski M 1906 Zur kinetischen Theorie der Brownschen Molekularbewegung und der Suspensionen *Annal. Phys., Lpz.* **326** 756–80

[257] Richardson L F 1926 Atmospheric diffusion shown on a distance-neighbour graph *Proc. R. Soc.* A **110** 709–37

[258] Tolić-Nørrelykke I, Munteanu E-L, Thon G, Oddershede L and Berg-Sørensen K 2004 Anomalous Diffusion in Living Yeast Cells *Phys. Rev. Lett.* **93** 078102

[259] Saxton M J 1994 Anomalous diffusion due to obstacles: a Monte Carlo study *Biophys. J.* **66** 394–401

[260] Saxton M J 1996 Anomalous diffusion due to binding: a Monte Carlo study *Biophys. J.* **70** 1250–62

[261] Metzler R and Klafter J 2000 The random walk's guide to anomalous diffusion: a fractional dynamics approach *Phys. Rep.* **339** 1–77

[262] Sokolov I M and Klafter J 2005 From diffusion to anomalous diffusion: a century after Einstein's Brownian motion *Chaos (Woodbury, NY)* **15** 26103

[263] Szymanski J and Weiss M 2009 Elucidating the origin of anomalous diffusion in crowded fluids *Phys. Rev. Lett.* **103** 038102

[264] Metzler R and Jeon J-H 2012 The role of ergodicity in anomalous stochastic processes: analysis of single-particle trajectories *Phys. Scr.* **86** 058510

[265] Bouchaud J-P and Georges A 1990 Anomalous diffusion in disordered media: Statistical mechanisms, models and physical applications *Phys. Rep.* **195** 127–293
[266] Meroz Y and Sokolov I M 2015 A toolbox for determining subdiffusive mechanisms *Phys. Rep.* **573** 1–29
[267] Scher H and Montroll E W 1975 Anomalous transit-time dispersion in amorphous solids *Phys. Rev.* B **12** 2455–77
[268] Mandelbrot B and Van Ness J 1968 Fractional Brownian motions, fractional noises and applications *SIAM Rev.* **10** 422–37
[269] Ernst D, Hellmann M, Kohler J and Weiss M 2012 Fractional Brownian motion in crowded fluids *Soft Matter* **8** 4886–9
[270] Mandelbrot B B 1983 *The Fractal Geometry of Nature* (London: Macmillan)
[271] Ben-Avraham D and Havlin S 2000 *Diffusion and Reactions in Fractals and Disordered Systems* (Cambridge: Cambridge University Press)
[272] Weiss M, Elsner M, Kartberg F and Nilsson T 2004 Anomalous subdiffusion is a measure for cytoplasmic crowding in living cells *Biophys. J.* **87** 3518–24
[273] Ben-Avraham D and Havlin S 1982 Diffusion on percolation clusters at criticality *J. Phys. A: Math. Gen.* **15** L691
[274] Saxton M J 2001 Anomalous subdiffusion in fluorescence photobleaching recovery: a Monte Carlo study *Biophys. J.* **81** 2226–40
[275] Cherstvy A G, Chechkin A V and Metzler R 2013 Anomalous diffusion and ergodicity breaking in heterogeneous diffusion processes *New J. Phys.* **15** 083039
[276] Dentz M and Bolster D 2010 Distribution-versus correlation-induced anomalous transport in quenched random velocity fields *Phys. Rev. Lett.* **105** 244301
[277] Chubynsky M V and Slater G W 2014 Diffusing diffusivity: a model for anomalous, yet Brownian, diffusion *Phys. Rev. Lett.* **113** 098302
[278] Kühn T, Ihalainen T O, Hyväluoma J, Dross N, Willman S F, Langowski J, Vihinen-Ranta M and Timonen J 2011 Protein diffusion in mammalian cell cytoplasm *PLoS One* **6** e22962
[279] Massignan P, Manzo C, Torreno-Pina J A, Garcia-Parajo M F, Lewenstein M and Lapeyre G J 2014 Nonergodic subdiffusion from Brownian motion in an inhomogeneous medium *Phys. Rev. Lett.* **112** 150603
[280] Golding I and Cox E 2006 Physical nature of bacterial cytoplasm *Phys. Rev. Lett.* **96** 098102
[281] Bronstein I, Israel Y, Kepten E, Mai S, Shav-Tal Y, Barkai E and Garini Y 2009 Transient anomalous diffusion of telomeres in the nucleus of mammalian cells *Phys. Rev. Lett.* **103** 018102
[282] He Y, Burov S, Metzler R and Barkai E 2008 Random time-scale invariant diffusion and transport coefficients *Phys. Rev. Lett.* **101** 058101
[283] Deng W and Barkai E 2009 Ergodic properties of fractional Brownian–Langevin motion *Phys. Rev.* E **79** 011112
[284] Barkai E 2008 *Theory and Evaluation of single-molecule signals* ed E Barkai *et al* (Singapore: World Scientific) pp 365–79 ch 11